Electronic Supplementary Material (ESI) for Dalton Transactions.
This journal is © The Royal Society of Chemistry 2020

The effect of isomerism and other structural variations on the G-quadruplex DNA-binding properties of some nickel schiff base complexes

Son Q.T. Pham,[a,b] Christopher Richardson,[a,b] Celine Kelso,[a,b] Anthony C. Willis[c] and Stephen F. Ralph[a,b]*

Supplementary Material

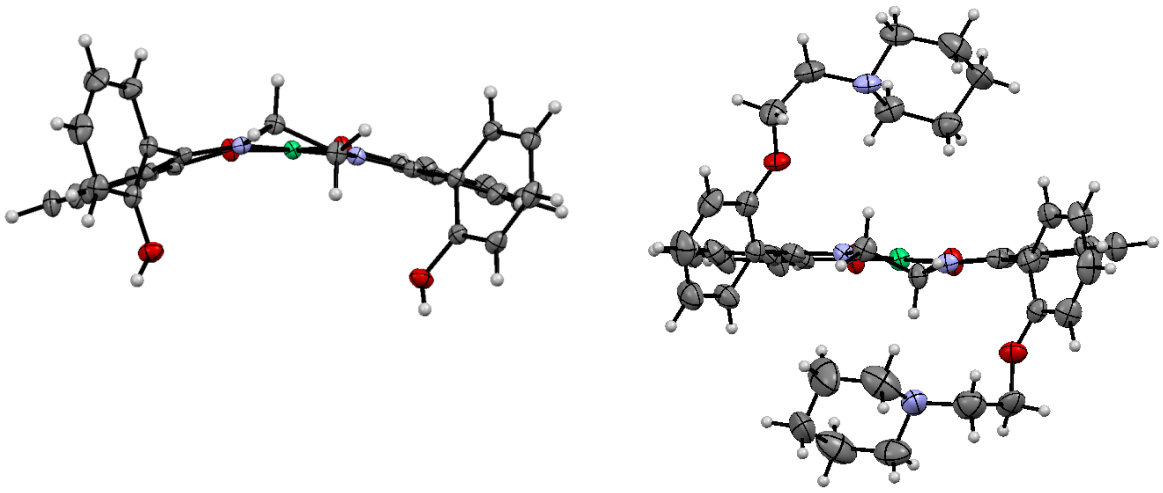

(a) (b)

Figure S1. Top view from the ethylenediamine moiety towards the metal centre of the crystal structures of **(5)** and **(6)**: (a) complex **(5)**; (b) complex **(6)**.

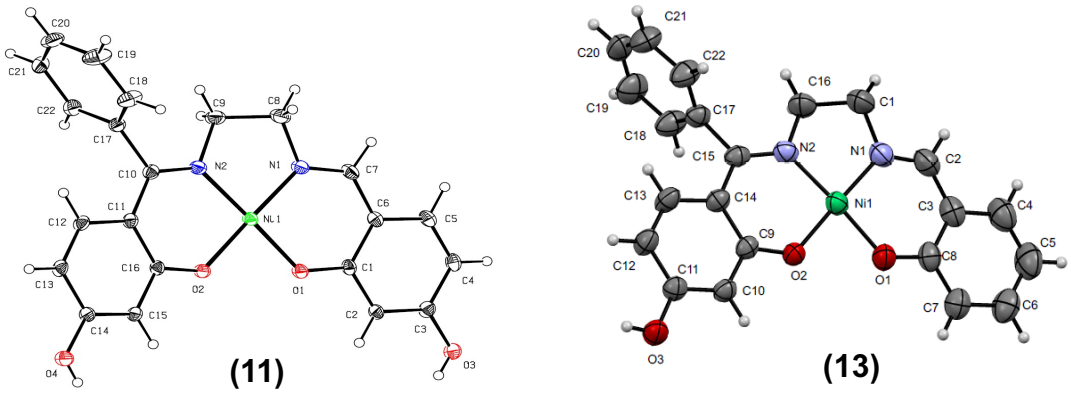

Figure S2. Molecular structures of **(11)** and **(13)**.

Table S1 Crystal data and structure refinement for complexes 3-6, 11.

Identification code	**3**	**4**	**5**	**6**	**11**
Empirical formula	$C_{31}H_{29}N_3NiO_5$	$C_{43}H_{48.96}Cl_3N_4NiO_{4.15}$	$C_{32}H_{34}N_2NiO_6S_2$	$C_{42}H_{48}N_4NiO_4$	$C_{22}H_{22}N_2NiO_6$
Formula weight	582.28	853.28	665.47	731.58	469.14
Temperature/K	294(1)	150.00(10)	150	150	150
Crystal system	monoclinic	triclinic	monoclinic	Triclinic	monoclinic
Space group	$P2_1/n$	P-1	$P2_1/c$	P-1	$P2_1/n$
a/Å	12.5896(2)	9.9317(3)	13.1465(1)	10.6471(4)	7.9887(1)
b/Å	17.1222(3)	14.6642(6)	14.9679(1)	26.9276(13)	20.7141(2)
c/Å	13.0803(3)	14.9018(5)	16.4141(2)	28.5309(16)	12.4586(2)
α/°	90	84.318(3)	90	65.563(5)	90
β/°	106.082(2)	76.970(3)	107.3576(11)	84.047(4)	98.9200(10)
γ/°	90	73.292(3)	90	83.883(3)	90
Volume/$Å^3$	2709.28(9)	2023.80(13)	3082.81(5)	7388.6(7)	2036.70(5)
Z	4	2	4	8	4
ρ_{calc}g/cm^3	1.428	1.400	1.434	1.315	1.530
μ/mm^{-1}	0.763	0.726	2.565	1.134	1.752
F(000)	1216.0	894.0	1392.0	3104.0	976.0
Crystal size/mm^3	0.40 × 0.31 × 0.25	0.46 × 0.13 × 0.10	0.369 × 0.217 × 0.036	0.306 × 0.077 × 0.032	0.132 × 0.084 × 0.029
Radiation	Mo Kα (λ = 0.71073)	Mo Kα (λ = 0.71073)	Cu Kα (λ = 1.54184)	Cu Kα (λ = 1.54184)	Cu Kα (λ = 1.54184)
2Θ range for data collection/°	3.974 to 58.26	3.962 to 57.4	7.044 to 148.032	6.286 to 143.87	8.356 to 147.418
Index ranges	-17 ≤ h ≤ 17, -23 ≤ k ≤ 23, -17 ≤ l ≤ 17	-13 ≤ h ≤ 13, -19 ≤ k ≤ 19, -20 ≤ l ≤ 20	-16 ≤ h ≤ 16, -18 ≤ k ≤ 18, -20 ≤ l ≤ 16	-12 ≤ h ≤ 9, -32 ≤ k ≤ 33, -35 ≤ l ≤ 33	-9 ≤ h ≤ 9, -25 ≤ k ≤ 25, -15 ≤ l ≤ 15
Reflections collected	60527	38950	35398	52284	31987
Independent reflections	7293 [R_{int} = 0.0491, R_{sigma} = 0.0293]	10295 [R_{int} = 0.0300, R_{sigma} = 0.0290]	6213 [R_{int} = 0.037]	27960 [R_{int} = 0.056]	4095 [R_{int} = 0.032]
Data/restraints/parameters	7293/112/414	10295/146/589	6213/0/394	27960/0/1838	4095/0/298
Goodness-of-fit on F^2	1.033	1.046	0.996	0.980	1.031
Final R indexes [I>=2σ (I)]	R_1 = 0.0421, wR_2 = 0.1042	R_1 = 0.0346, wR_2 = 0.0846	R_1 = 0.0362, wR_2 = 0.0974	R_1 = 0.0968, wR_2 = 0.1772	R_1 = 0.0381, wR_2 = 0.0954
Final R indexes [all data]	R_1 = 0.0684, wR_2 = 0.1214	R_1 = 0.0452, wR_2 = 0.0890	R_1 = 0.0381, wR_2 = 0.0993	R_1 = 0.1262, wR_2 = 0.1945	R_1 = 0.0412, wR_2 = 0.0975
Largest diff. peak/hole / e $Å^{-3}$	0.51/-0.55	0.43/-0.28	1.21/-0.54	1.36/-0.76	0.88/-0.50
Flack Parameter	N/A	N/A	N/A	N/A	N/A
CCDC Number	1984622	1984623	1988290	1988291	1988292

Table S2 Crystal data and structure refinement for 13, 15-16.

Identification code	**13**	**15**	**16**
Empirical formula	$C_{22}H_{19}N_2NiO_{3.5}$	$C_{26}H_{22}N_2NiO_4$	$C_{33}H_{33}N_3NiO_3$
Formula weight	426.10	485.16	578.33
Temperature/K	294(1)	150.00(10)	150.00(10)
Crystal system	monoclinic	monoclinic	monoclinic
Space group	$P2_1/c$	Cc	$P2_1$
a/Å	10.3061(3)	13.4737(3)	18.9200(4)
b/Å	20.2032(5)	18.9348(3)	7.61382(12)
c/Å	9.6204(3)	8.4020(2)	19.7486(3)
α/°	90	90	90
β/°	106.606(3)	101.792(2)	99.5135(16)
γ/°	90	90	90
Volume/$Å^3$	1919.58(10)	2098.30(8)	2805.73(8)
Z	4	4	4
ρ_{calc}g/cm^3	1.474	1.536	1.369
μ/mm^{-1}	1.039	0.963	0.731
F(000)	884.0	1008.0	1216.0
Crystal size/mm^3	0.50 × 0.21 × 0.05	0.47 × 0.27 × 0.05	0.4 × 0.25 × 0.13
Radiation	Mo Kα (λ = 0.71073)	Mo Kα (λ = 0.71073)	Mo Kα (λ = 0.71073)
2Θ range for data collection/°	4.032 to 56.558	5.696 to 57.54	4.182 to 57.394
Index ranges	$-13 \le h \le 13$, $-26 \le k \le 26$, $-12 \le l \le 12$	$-18 \le h \le 18$, $-25 \le k \le 25$, $-9 \le l \le 11$	$-25 \le h \le 25$, $-10 \le k \le 10$, $-26 \le l \le 25$
Reflections collected	40482	21869	73796
Independent reflections	4762 [R_{int} = 0.0379, R_{sigma} = 0.0246]	4964 [R_{int} = 0.0334, R_{sigma} = 0.0235]	14383 [R_{int} = 0.0266, R_{sigma} = 0.0229]
Data/restraints/parameters	4762/3/269	4964/2/302	14383/1/721
Goodness-of-fit on F^2	1.049	1.062	1.032
Final R indexes [I>=2σ (I)]	R_1 = 0.0327, wR_2 = 0.0800	R_1 = 0.0256, wR_2 = 0.0672	R_1 = 0.0307, wR_2 = 0.0784
Final R indexes [all data]	R_1 = 0.0467, wR_2 = 0.0868	R_1 = 0.0269, wR_2 = 0.0680	R_1 = 0.0357, wR_2 = 0.0811
Largest diff. peak/hole / e $Å^{-3}$	0.26/-0.30	0.31/-0.24	0.54/-0.30
Flack Parameter	N/A	-0.012(6)	-0.011(5)
CCDC Number	1984624	1984625	1984626

Complex 3

Data for (**3**) was collected at room temperature using Mo Kα radiation. One full nickel complex crystallises with a DMF solvate molecule in the asymmetric unit of the space group $P2_1/n$. All CH hydrogens and OH hydrogens are refined under riding models in idealized positions with fixed Uiso (1.2 times for C(H) and C(H,H) groups; at 1.5 times C(H,H,H) groups and O(H) groups). The disorder in the ethylenediamine bridge modelled as two component disorder with largest occupancy 0.52 with restrained distances for N-C bonds (1.48(0.02) Å) and C-C bonds (1.51(0.02) Å). The disordered DMF solvate was modelled as a two component disorder with largest occupancy 0.60 and with planarity and rigid body restraints over both components as well as same distance restraints and distance-angle restraints. The thermal ellipsoids of O3AA and C5D are rather large and were left as is considering this is a disordered solvate atom hydrogen bonded to the complex.

Complexes assemble in the slipped cofacial association with three types of notable interaction shown in Figure S3 (only the major part of the disorder shown). The complexes assemble into chains through hydrogen bonds (O17-H17---O16P 1.917(2) Å) that orientate the hydrogen-bonded polymeric structure to run parallel to the *b*-axis direction. The chains are in close contacts via the slipped cofacial interactions and the DMF molecules lie in spaces between chains.

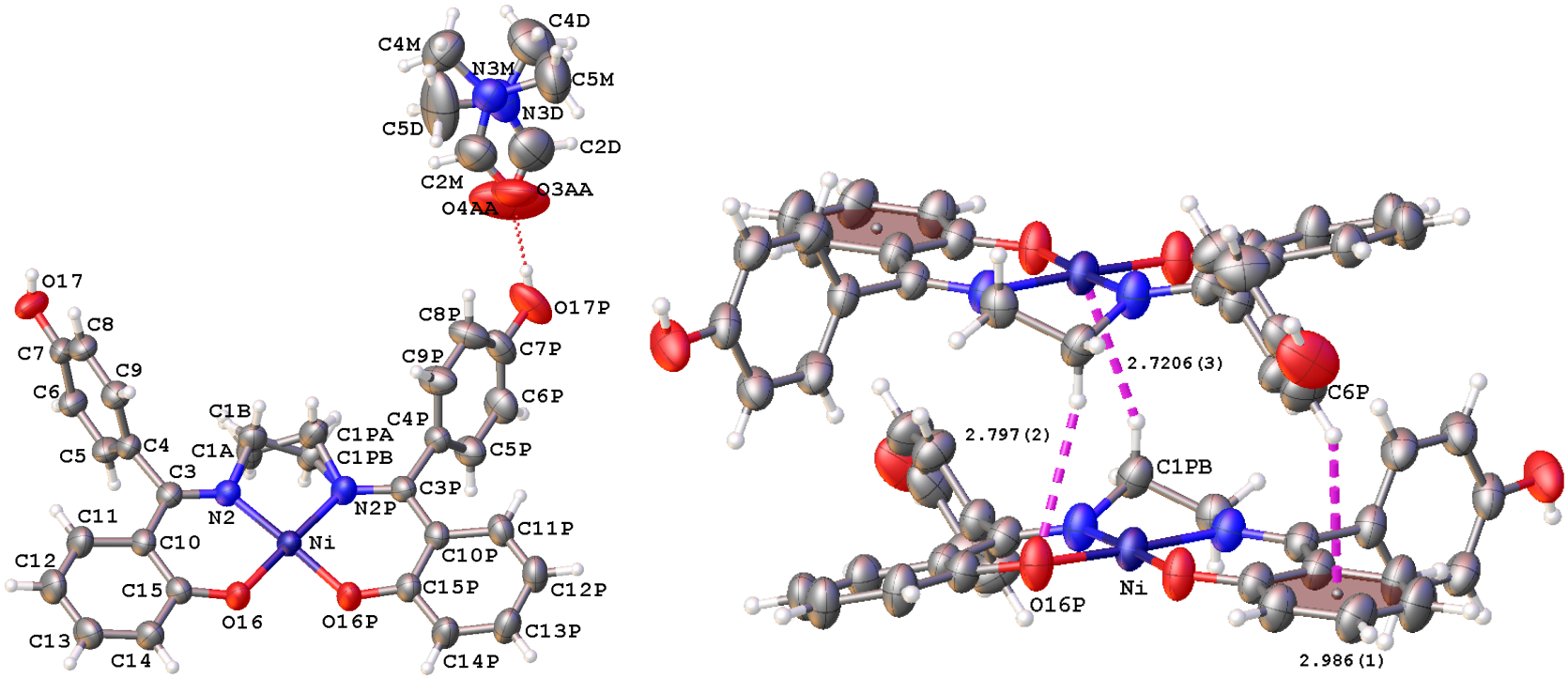

Figure S3. The contents of the asymmetric unit of (**3**) (left) and the interactions in the slipped co-facial positioning in the structure of (**3**)(right).

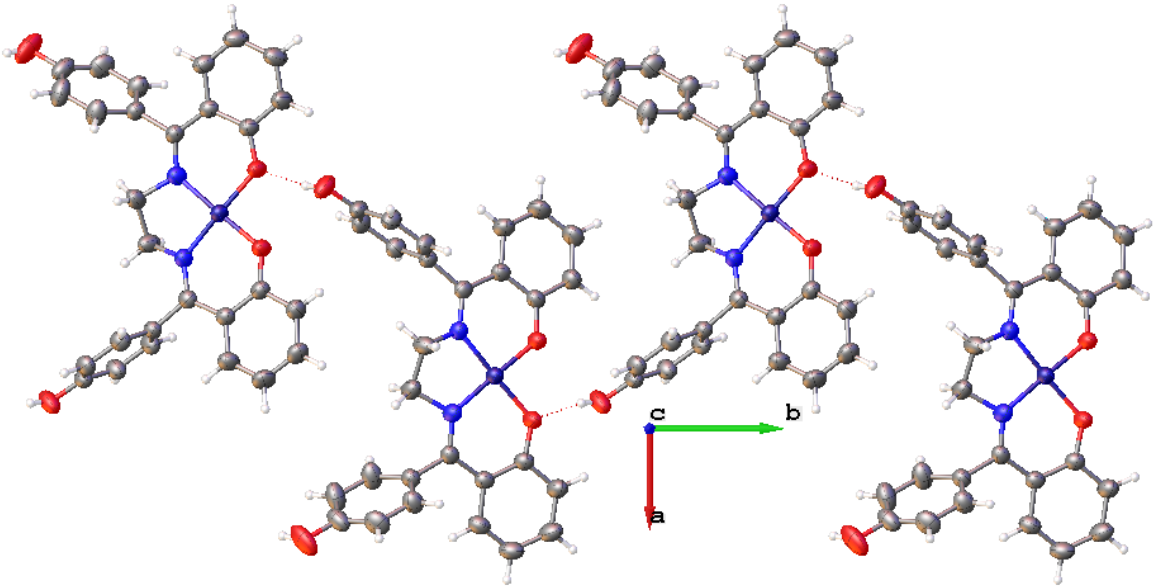

Figure S4. The hydrogen-bonded polymeric structure of (**3**) running parallel to the crystallographic *b*-axis.

Complex 4

The data for (**4**) was collected at 150 K using Mo Kα radiation. The asymmetric unit in the triclinic space group $P\bar{1}$ contains one metal complex, one chloroform solvate and a partial occupancy water molecule that makes a sensible D-A contact with a piperidinyl nitrogen atom (Figure S5). Free refinement of the occupancy of the water came to ca. 0.15 and it was fixed at that. The position of this low occupancy water did not refine well (FMLS did not converge), so its position was fixed therefore the distance and relationship of this interaction was not taken further. The ethylenediamine chelate ring is disordered over two positions (90:10) and the chloroform solvate molecule is also disordered over two positions (0.57:0.43). The distances around the chelate ring were restrained to be approximately the same and the thermal parameters for C1 and C1A were constrained to be identical. One of the complex's piperidine termini is disordered over two positions (0.83:17). This was modelled using the SAME restraint and several of the ADP in the lower-occupancy ring were made the same as the major position. C22A was included in the refinement with a strong ISOR restraint. All hydrogen atoms are idealized in position in riding models on their carrier atoms. One DFIX restraint was necessary for a pair of C-Cl bonds (Cl1A and Cl1B).
The supramolecular structure of this complex is discussed in the main text of the article.

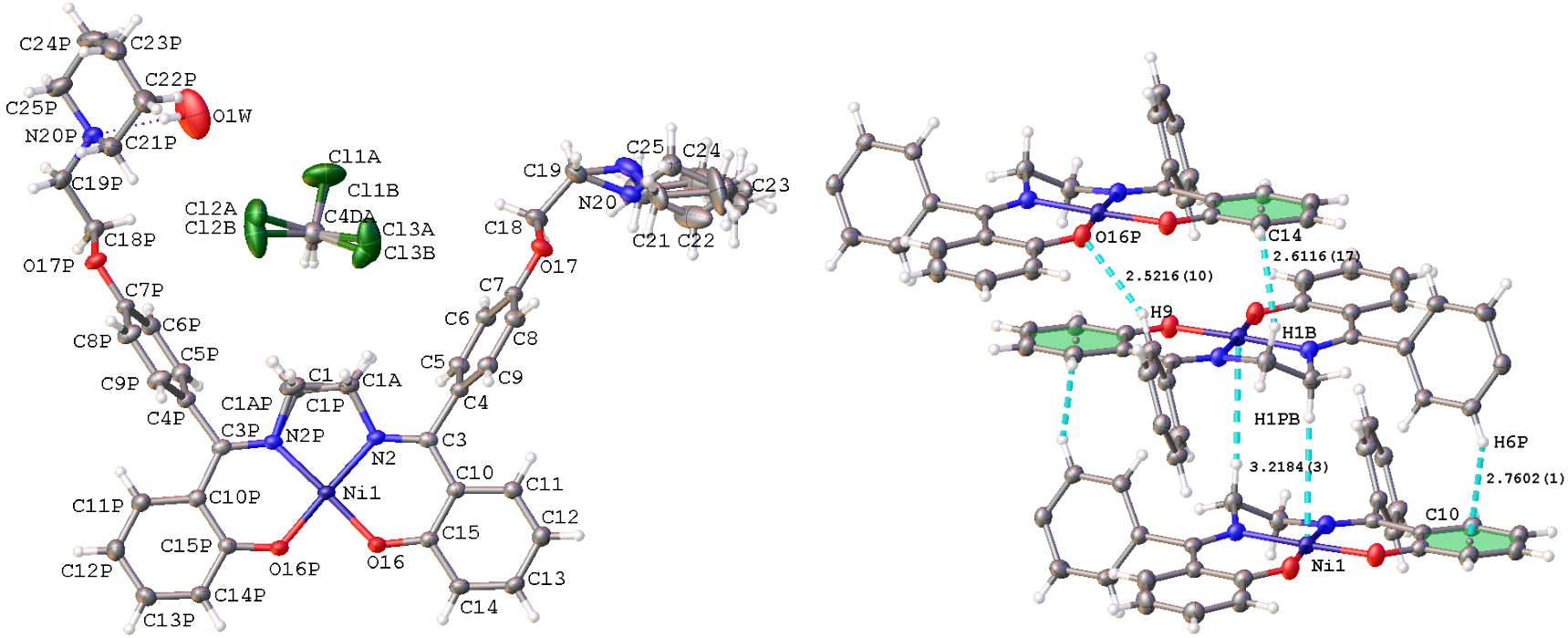

Figure S5. The contents of the asymmetric unit of (**4**) (left) and the two pairwise interactions found in the structure of (**4**)(right). The pendant ethoxypiperidinyl arms have been removed for clarity in the structure at right.

Complex 5

Data was collected at 150 K using Cu Kα radiation. Complex (**5**) crystallised from DMSO solution as a disolvate with a full complex in the asymmetric unit in the monoclinic space group $P2_1/c$ (Figure S6). The refinement was unrestrained with all hydrogen atom positions refined. The largest features in the final difference electron density map of **(5)** were located near S2 and midway between bonded C atoms. Each DMSO molecule is hydrogen-bonded to a hydroxyl group of the complex [O3-H3---O6 1.76(3) Å ; O4-H4---O5 1.85(3) Å] with both hydroxyl groups found on the same face relative to the square planar N_2O_2 coordination geometry. Complexes assemble in a 'back-to'back' fashion over a centre of inversion with the closest intermolecular distance between an axial hydrogen of a $-CH_2$ group and the π system of the partner complex [H81---C16 2.699(2) Å], as shown in Figure S6. With all hydrogen bonds satisfied by the DMSO molecules, complexes are not connected further and are essentially isolated dimers within the structure. When viewed parallel to the *a*-axis, channels filled by the DMSO molecules are apparent.

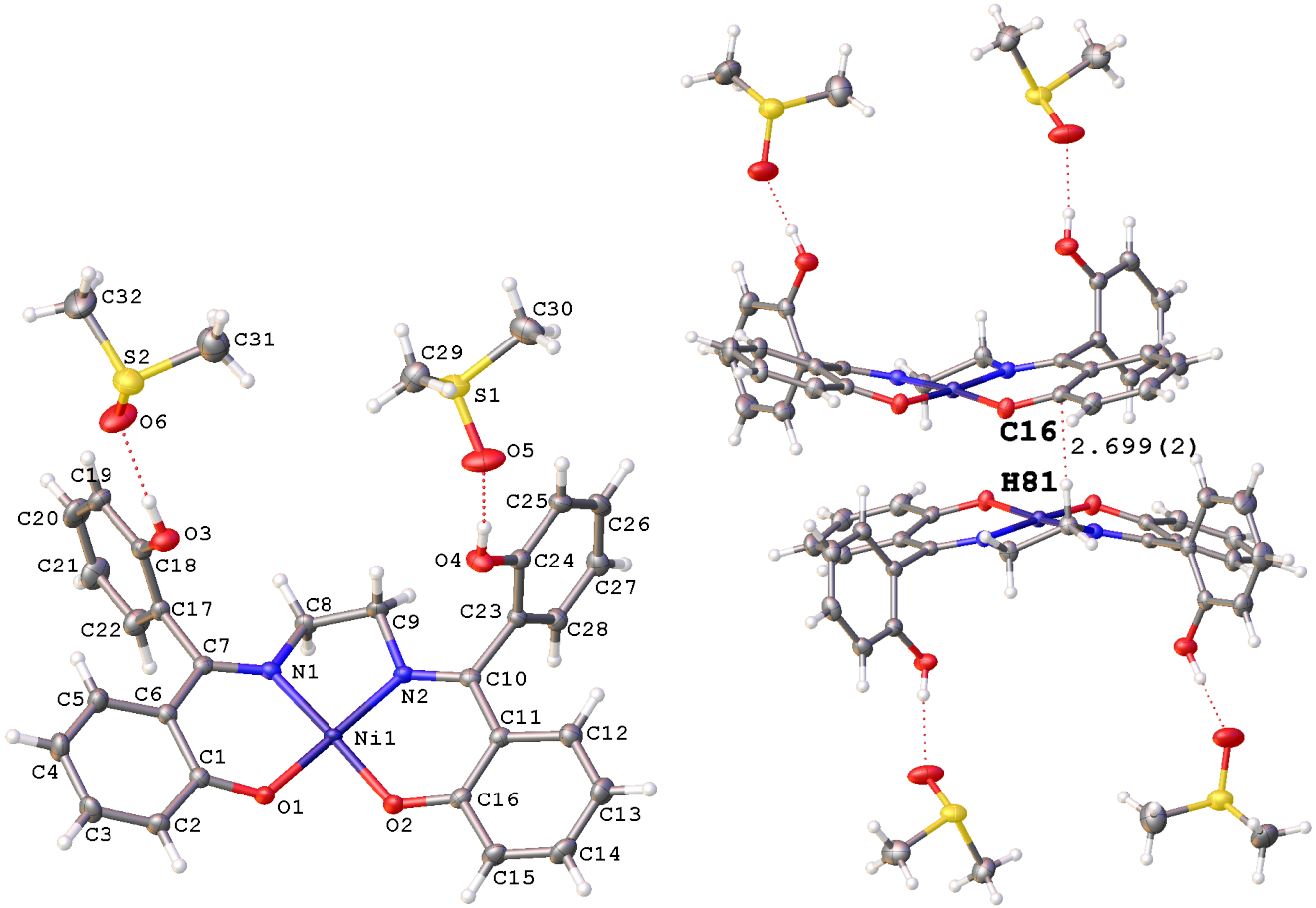

Figure S6. The contents of the asymmetric unit of (**5**) (left) and a view of the dimeric association about an inversion centre in the lattice of (**5**)(right).

Complex 6

Data was collected at 150 K using Cu Kα radiation. The asymmetric unit in the triclinic space group $P\overline{1}$ contains four very slightly different complexes. Details of the structure are discussed in the main text of the article. The C-H---N distances for the four complexes are: [N3---H482 2.511(7) Å; N4---H491 3.308(4) Å], [N7---H582 3.241(4) Å; N8---H591 2.538(7) Å], [N11---H108 2.674(5) Å; N12---H2 2.950(6) Å], [N16---H1b---N16 2.665(5) Å; N15---H158 2.839(7) Å]. During refinement of (**6**), H atoms were included at calculated positions and allowed to ride on the atoms to which they were bonded. The program PLATON was used to examine the structure and its data, and it suggested a twinning operation which would aid the refinement. Application of this twinning correction within CRYSTALS gave a significant improvement in the agreement factors. The largest features in the final difference electron density map were located near Ni atoms.

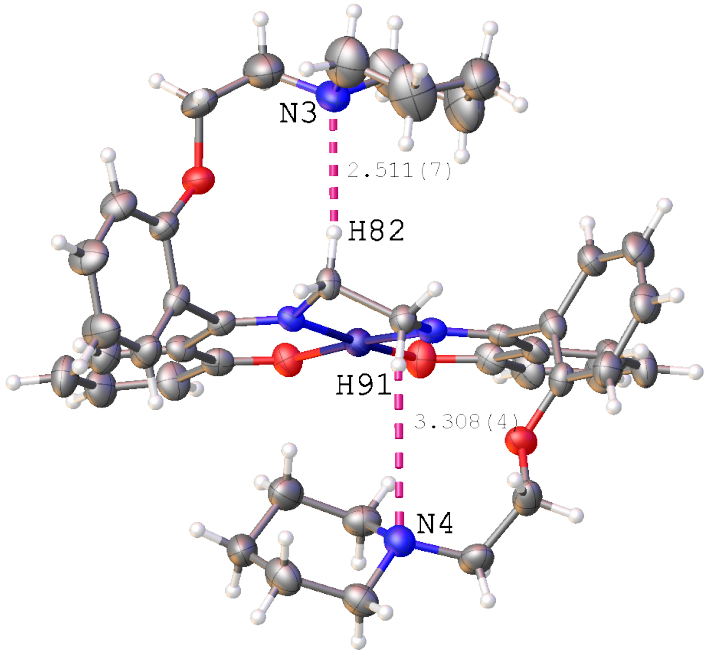

Figure S7. A view displaying the C-H---N interactions of one of the complexes in the asymmetric unit of (**6**).

Complex 11

Data for (**11**) were collected at 150 K using Cu Kα radiation. Crystals formed from a methanol/DMSO solution and one full molecule that hydrogen bonds to two water molecules crystallises in the asymmetric unit of $P2_1/n$, as shown in Figure S8. The structure was refined with no restraints. The H atoms were all located in a difference map, but those bonded to C were repositioned geometrically. The H atoms were initially refined with soft restraints on the bond lengths and angles to regularise their geometry (C-H in the range 0.93--0.98 Å, O-H = 0.83 Å) and with Uiso(H) in the range 1.2-1.5 times Ueq of the parent atom, after which the positions were refined with riding constraints and the displacement parameters were held fixed. Finally the positions of the H atoms bonded to O were allowed to refine freely. The largest feature in the final difference electron density map is located near C3 and C4 but appears to have no chemical significance. The next largest features are near O2, C3 and the Ni atom.

The slipped cofacial association is not present as complexes do not crystallise as pairs about inversion centres. The supramolecular structure is dominated by hydrogen bonding between water molecules and hydroxyl groups of **11**. A full list of hydrogen bonding distances and angles is provided in the table below. Each water is a hydrogen bond donor to two complexes [O5-H3---O2; O5-H4---O4 (-1+X,+Y,+Z)] [O6-H5---O1; O6-H6---O3 (1+X,+Y,+Z)] with the latter D-A contacts to terminal hydroxyl groups of other complexes, thus hydrogen bonded chains that propagate along the *a*-axis direction are formed. The water molecules then act as a 3-connecting node by accepting hydrogen bonds and forming cross-links in the *b*-axis direction to another chain, so that a hydrogen-bridged tape is formed. Helping to orientate the complexes in the chains along the *a*-axis direction are π-π interactions (~3.52 Å) between the different ends of the asymmetric complex (Figure S8).

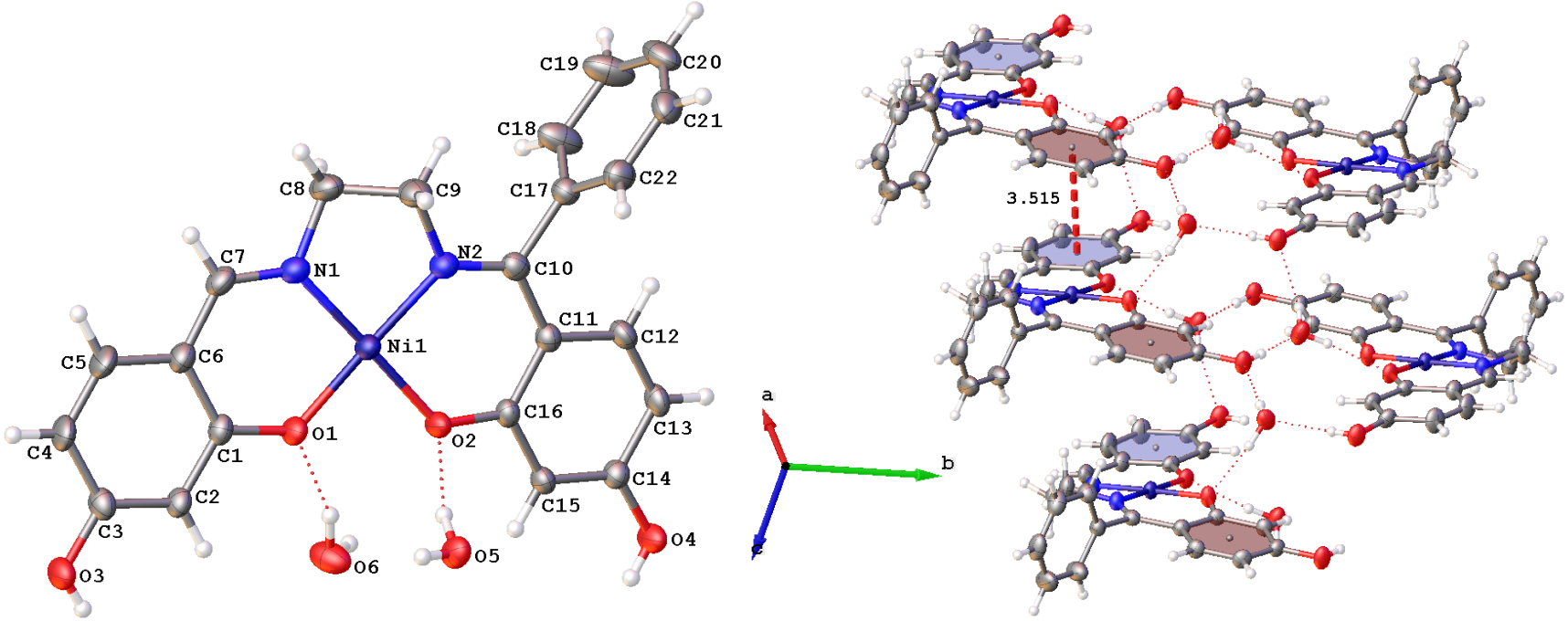

Figure S8. The contents of the asymmetric unit of (**11**) (left) and a perspective view of a part of one hydrogen-bonded tape in the lattice.

Table S3 Hydrogen Bonds for (11).

D	H	A	D-H-A/°	d(D-H)/Å	d(H-A)/Å	d(D-A)/Å
O3	H1	O5[1]	171(3)	0.74(3)	1.90(3)	2.634(3)
O4	H2	O6[2]	175(3)	0.75(3)	1.82(3)	2.566(3)
O5	H3	O2	167(3)	0.88(3)	1.88(3)	2.742(3)
O5	H4	O4[3]	179(4)	0.71(3)	2.05(3)	2.761(3)
O6	H5	O1	161(3)	0.85(4)	1.98(4)	2.790(3)
O6	H6	O3[4]	163(3)	0.80(4)	2.10(4)	2.878(3)

[1]-X,-Y,1-Z; [2]1-X,-Y,1-Z; [3]-1+X,+Y,+Z; [4]1+X,+Y,+Z

Complex 13

Data were collected at 294 K using Mo Kα radiation. One molecule and a partial occupancy (50%) water make up the asymmetric unit of this structure in the monoclinic space group $P2_1/c$ (Figure S9). The O1W-O1 hydrogen bond is a very long contact at 2.11(5) Å and this water seems to make no other definitive contacts and needed to be modelled with restraints for the distances and angles of the hydrogens. Complexes do assemble over inversion centres in what we refer to as a 'slipped cofacial' configuration. In (**13**) this leads to a very short Ni-Ni distance of 3.4224(7) Å but the shorter contacts are between hydrogens of the ethylenediamine chelate rings and the coordinating oxygens of the partner complex [H1A---O2 2.613(1) Å], which we commonly see as the closest interaction (Figure S9). The [C17-C22-C21-C20-C19-C18] to [Ni-N2-C15-C14-C9-O2] plane twist angle is 88.64(7)° and the former phenyl ring distinctly angles away to make room for a C-H-π contact between H22 and C7 [2.728(2) Å]. In the supramolecular structure of (**13**), there is an intermolecular hydrogen-bonded chain [O2AA-O2 1.919(1) Å] that propagates along the *c*-direction (Figure S9).

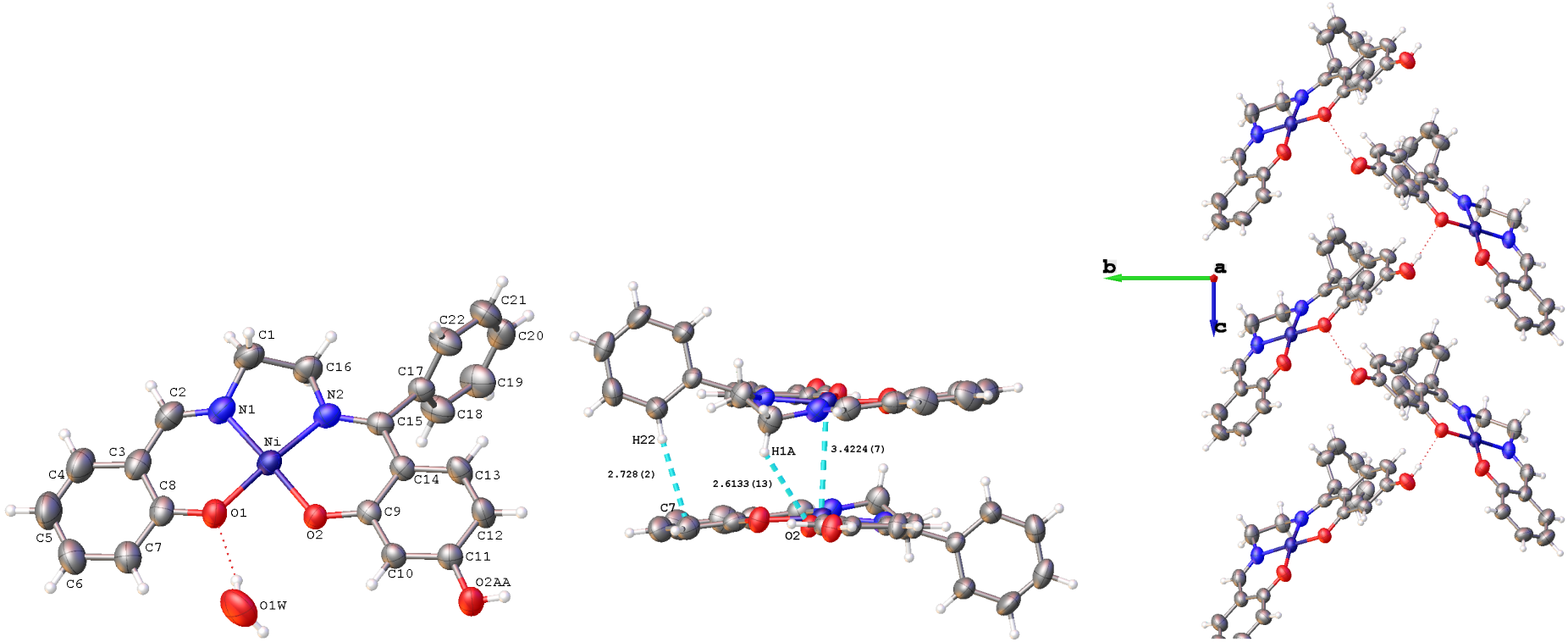

Figure S9. The contents of the asymmetric unit of (**13**) (left); a view of the interactions in the slipped cofacial configuration (middle); a view of a portion of the hydrogen-bonded polymeric chain propagating along the crystallographic *c*-direction.

Complex 15

Data were collected at 150 K using Mo Kα radiation. One metal complex hydrogen bonded to a water molecule makes up the asymmetric unit of this structure in the monoclinic space group *Cc* (Figure S10). The data statistics clearly pointed to acentric and the data refines well and gives an acceptable Flack parameter (Flack x: -0.012(6); Hooft y: -0.009(3)). PLATON did not suggest additional symmetry. The hydrogens attached to carbon were refined in riding models with fixed Uiso values. The water was refined as a freely rotating group as was the hydrogen attached to the phenolic group. Table S4 gives the distance and angular parameters for the hydrogen bonding in the structure. Not unlike complex **(11)**, the assembly of the structure is dominated by the lattice water acting as a 3-connecting node (Figure S10): O1W acts as an acceptor to H4 (H4---O1W 1.8319(17) Å) and a donor to $O4^{i}$ (+X,1-Y,-1/2+Z) [H1WA---$O4^{i}$ 2.1502(17) Å] and $O2^{ii}$ (+X,1-Y,1/2+Z) [H1WB---$O2^{ii}$ 2.0292(16) Å]. The latter two interactions are supported by π-π stacking interactions from the napthyl ring system of one complex to the planar chelate ring (Ni1-O2-C2-C1-C7-N1; fold angle 4.62(7)°) and its attached phenolic ring (fold angle 6.44(8)°) of another complex. The water molecules, aided by the stacking interactions aligning the aromatic rings, bring chains of complexes together, forming hydrogen-bonded tapes running along the *c*-axis direction (Figure S10).

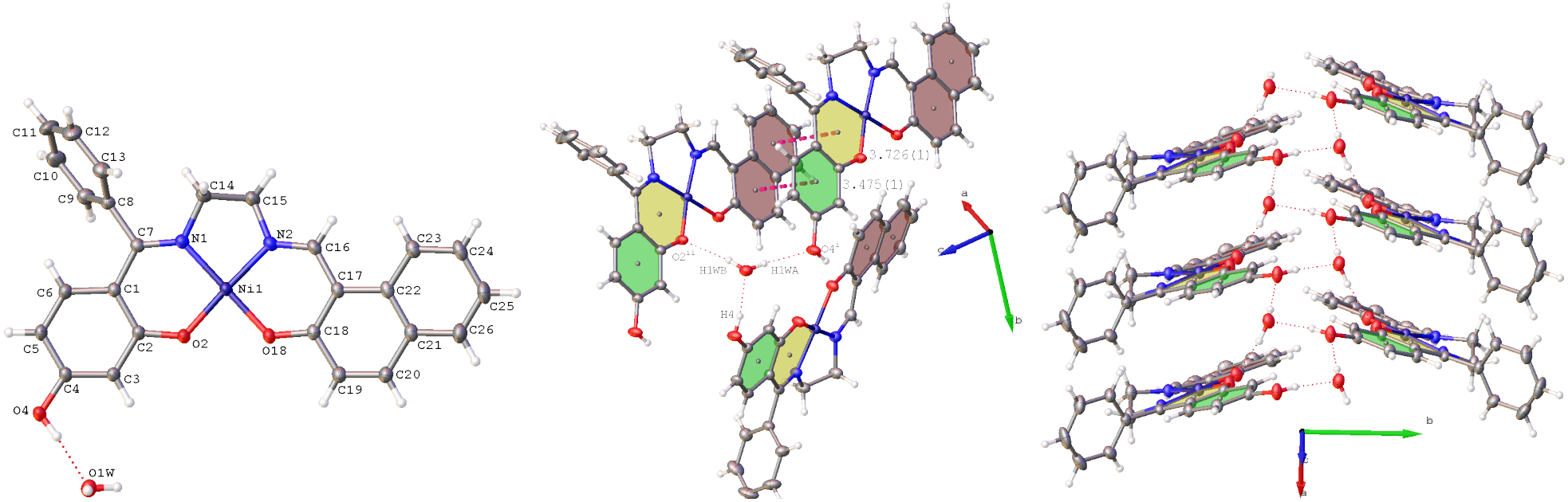

Figure S10. The contents of the asymmetric unit of (**15**) (left); a view displaying the 3-connecting nature of O1W and the intermolecular π-stacking between napthyl and chelate rings (middle); a view slightly offset from the *c*-axis of a part of a hydrogen-bonded tape structure in the crystal lattice of (**15**)(right).

Table S4 Hydrogen Bonds for (15).

D	H	A	d(D-H)/Å	d(H-A)/Å	d(D-A)/Å	D-H-A/°
O4	H4	O1W	0.82	1.83	2.647(2)	172.3
O1W	H1WB	O2[1]	0.85	2.03	2.816(3)	153.4

[1]+X,1-Y,1/2+Z

Complex 16

Data were collected at 150 K using Mo Kα radiation. Two different complexes crystallise in the asymmetric unit of the monoclinic space group $P2_1$. The data statistics pointed to acentric and the data refines well with an acceptable Flack parameter (Flack x: -0.011(5); Hooft y: -0.). PLATON did not suggest additional symmetry and refinement was unsuccessful in centrosymmetric monoclinic space groups (e.g. $P2_1/c$). All non-hydrogen atoms were freely refined. The hydrogens attached to carbon were refined in riding models with fixed Uiso values. The largest feature in the difference map indicated some evidence for disorder of one piperidine ring but pursuing this did not lead to worthwhile improvement as the component was ~ 6-7%. The structure is discussed in more detail in the main article text.

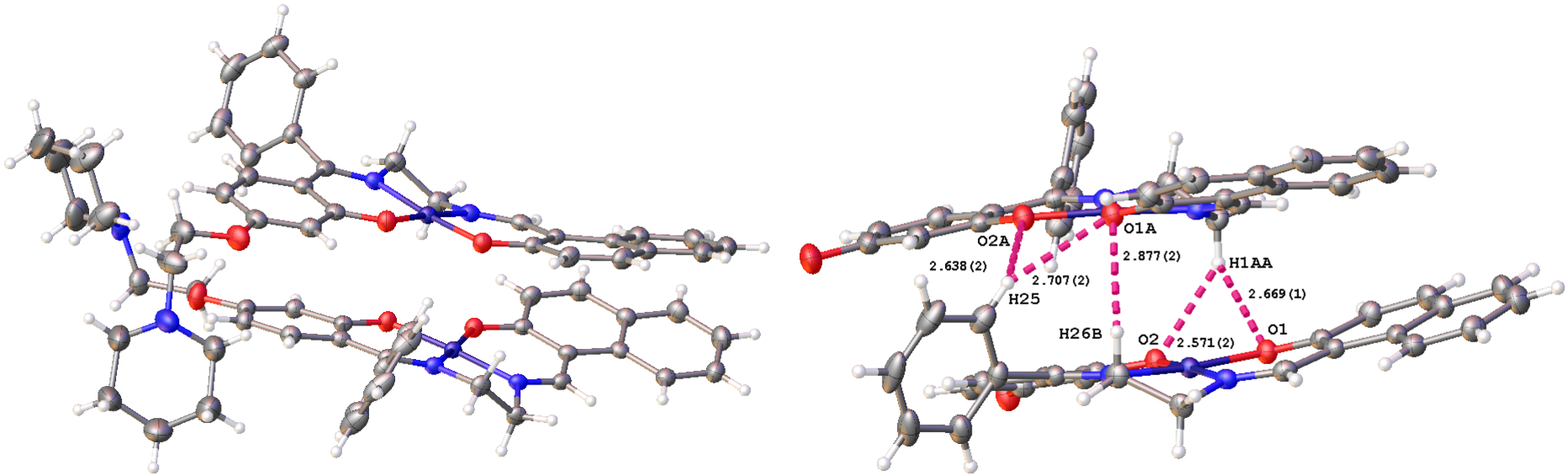

Figure S11. The two complexes in the asymmetric unit of (**16**). No labelling for clarity (left); A view displaying the close contacts between the two complexes in the asymmetric unit, with piperidinylethyl groups removed for clarity (right).

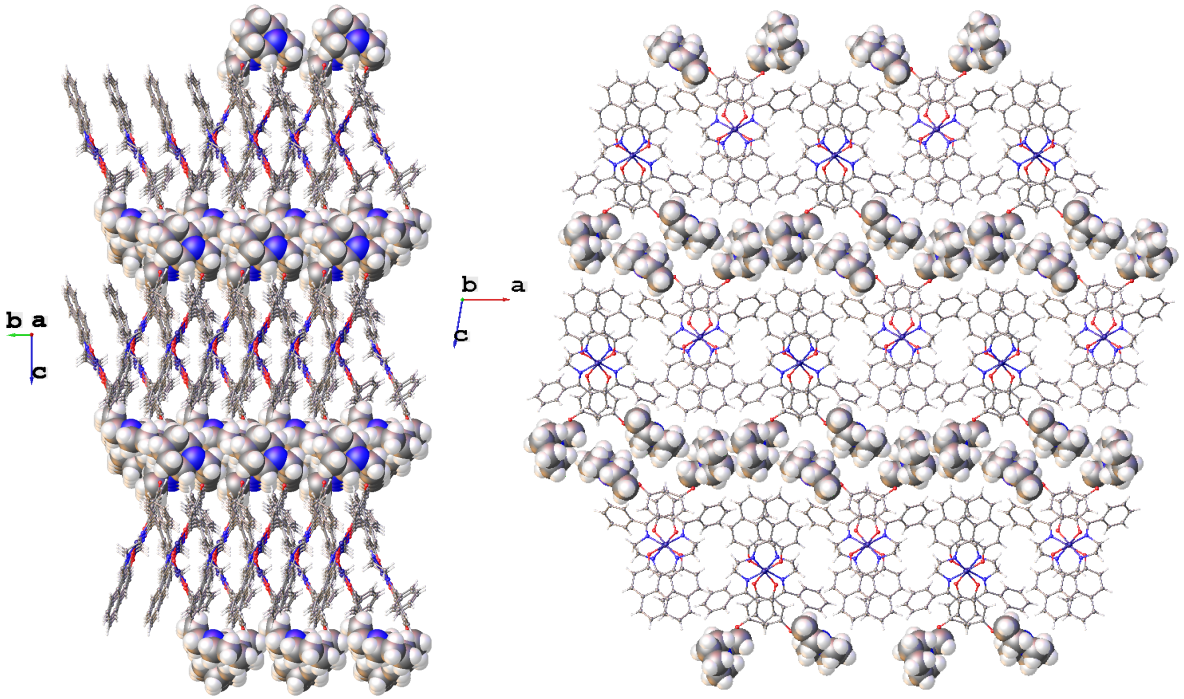

Figure S12. Views parallel to the *a*-axis (left) and *b*-axis (right) showing the channels the piperidinyl groups (shown in space filling form) occupy in the supramolecular structure of (**16**).

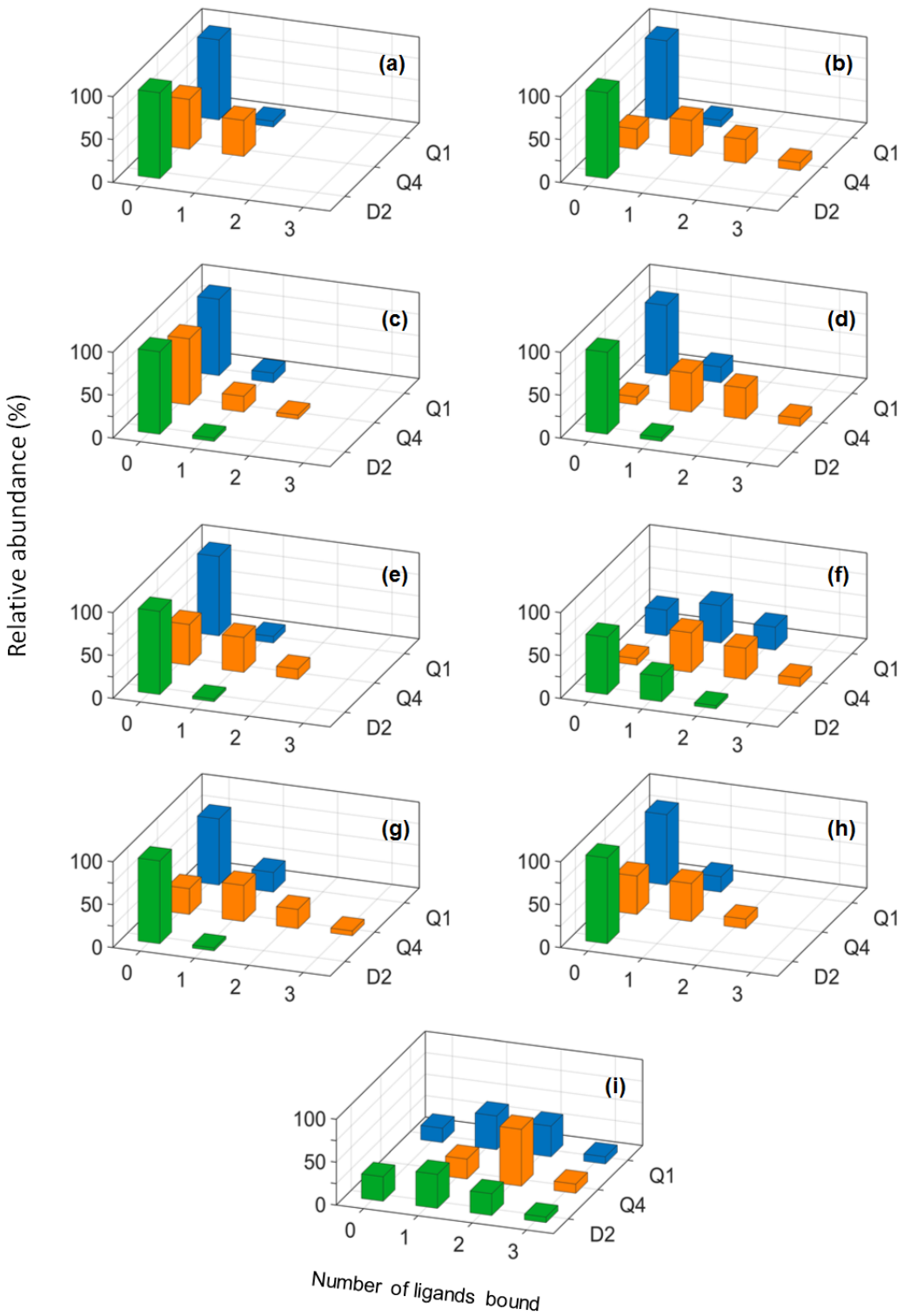

Figure S13. Relative abundances of ions in ESI mass spectra of solutions containing a 6:1 ratio of nickel Schiff base complexes and dsDNA (D2), unimolecular qDNA (Q1) or tetramolecular qDNA (Q4): (a) solutions containing **(2)**; (b) solutions containing **(4)**; (c) solutions containing **(6)**; (d) solutions containing **(8)**; (e) solutions containing **(10)**; (f) solutions containing **(12)**; (g) solutions containing **(14)**; (h) solutions containing **(16)** and (i) solutions containing **(1)**. Data for complexes **(1)** and **(2)** taken from reference 18 in the main manuscript.

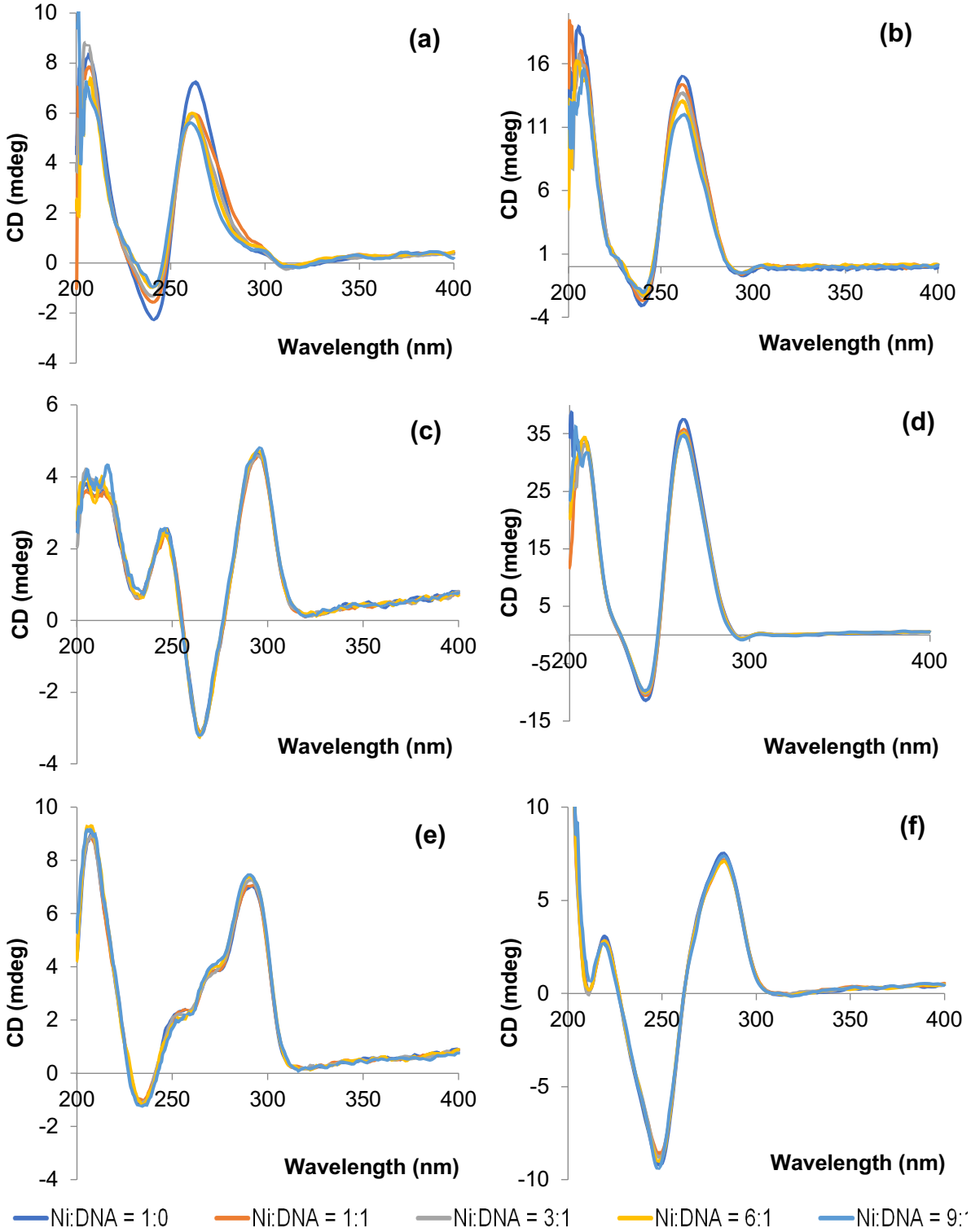

Figure S14a. Circular dichroism spectra of solutions containing different ratios of **(6)** and various DNA: (a) Parallel Q1 + **(6)**; (b) Parallel c-kit1 + **(6)**; (c) Anti-parallel Q1 + **(6)**; (d) Parallel Q4 + **(6)**; (e) Hybrid-type 1 Q1 + **(6)**; (f) D2 + **(6)**.

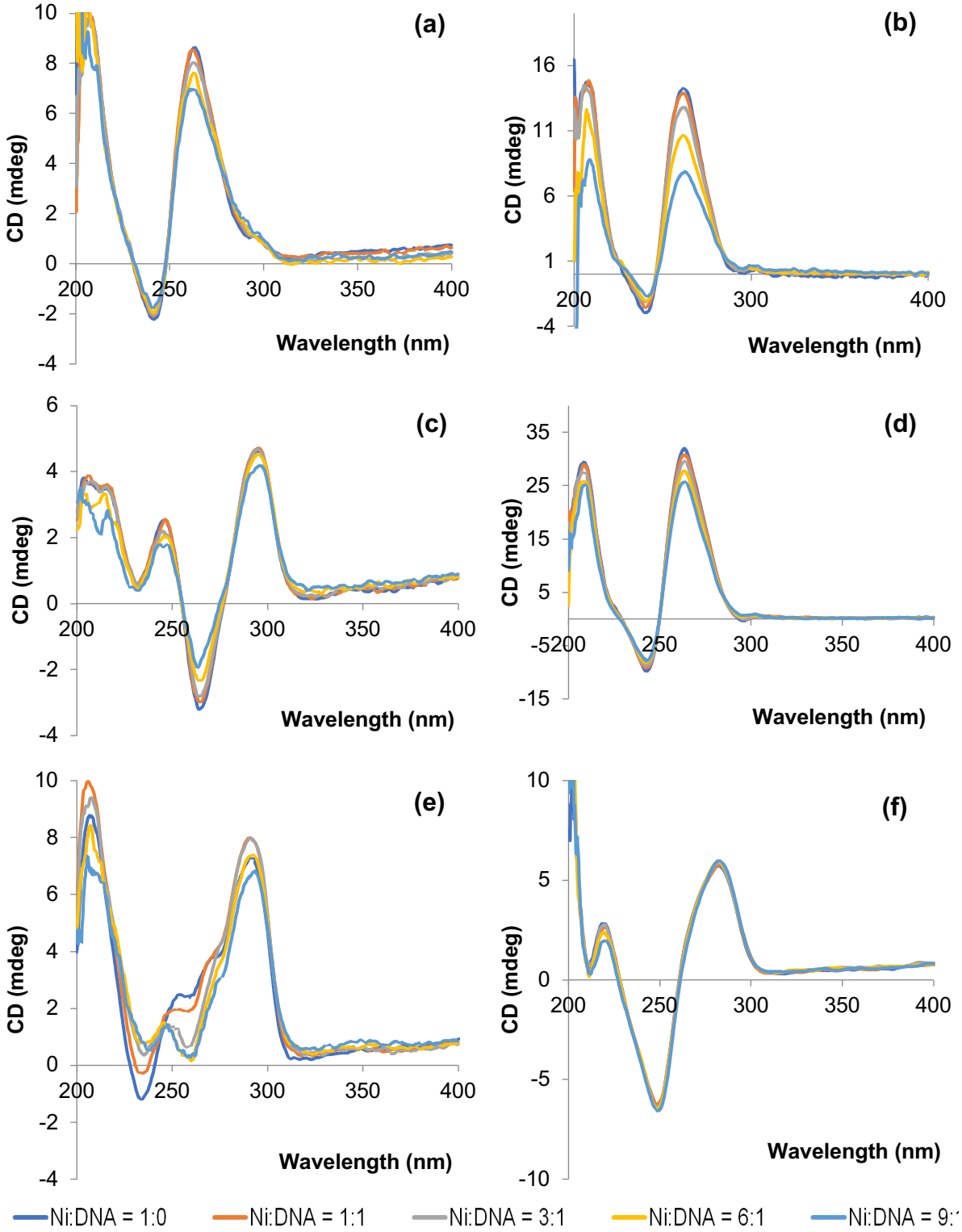

Figure S14b. Circular dichroism spectra of solutions containing different ratios of **(8)** and various DNA: (a) Parallel Q1 + **(8)**; (b) Parallel c-kit1 + **(8)**; (c) Anti-parallel Q1 + **(8)**; (d) Parallel Q4 + **(8)**; (e) Hybrid-type 1 Q1 + **(8)**; (f) D2 + **(8)**.

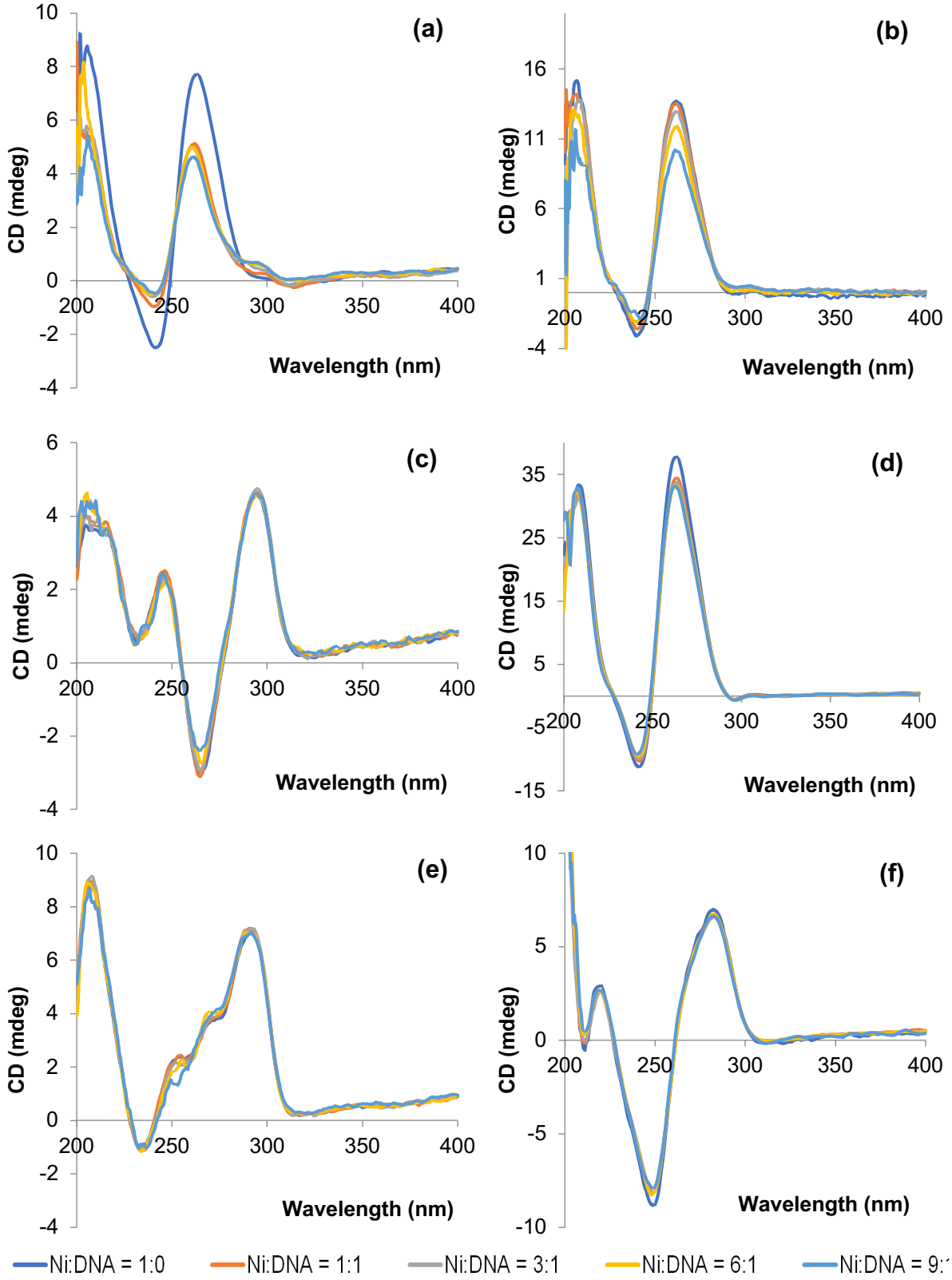

Figure S14c. Circular dichroism spectra of solutions containing different ratios of **(10)** and various DNA: (a) Parallel Q1 + **(10)**; (b) Parallel c-kit1 + **(10)**; (c) Anti-parallel Q1 + **(10)**; (d) Parallel Q4 + **(10)**; (e) Hybrid-type 1 Q1 + **(10)**; (f) D2 + **(10)**.

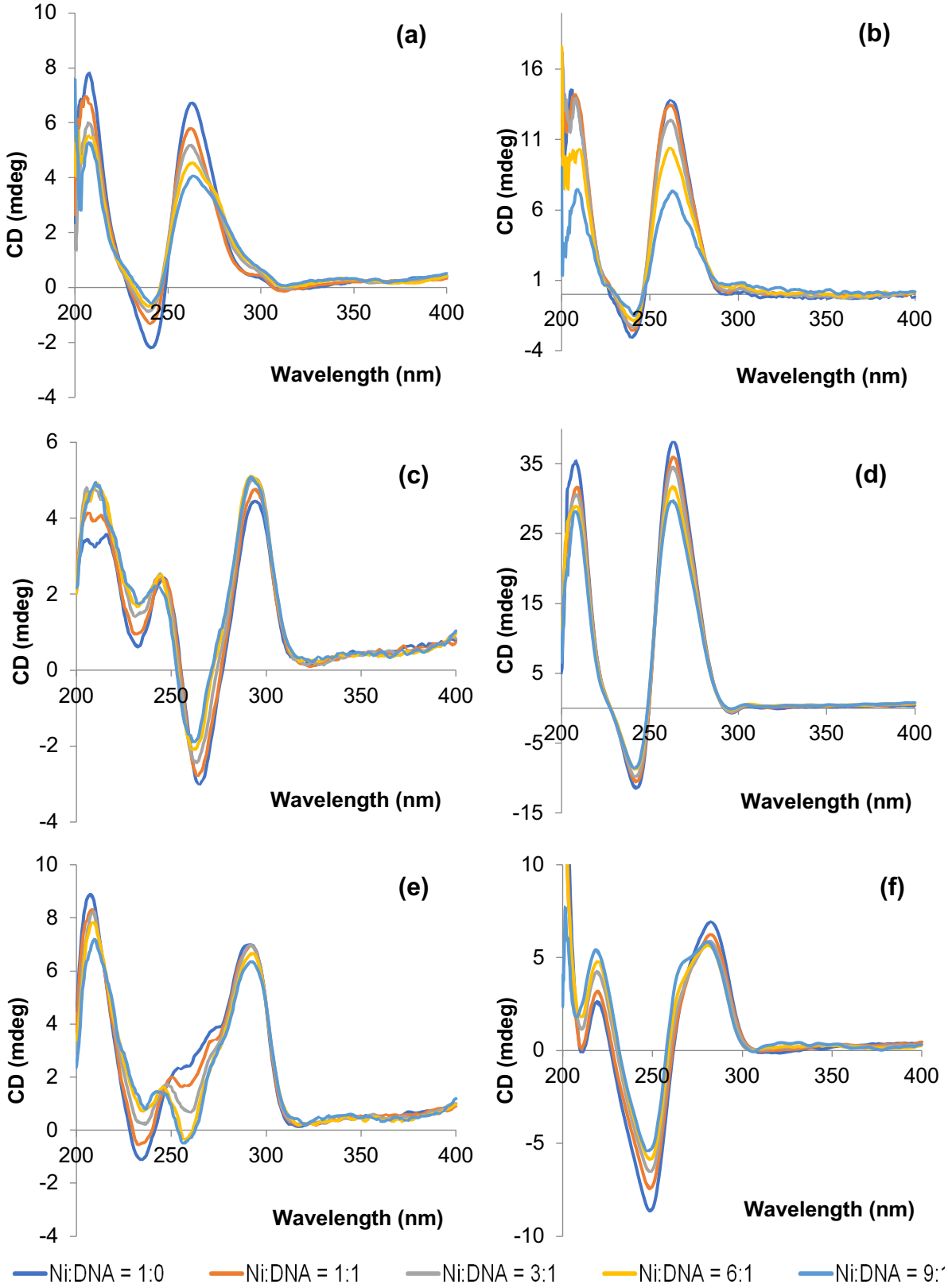

Figure S14d. Circular dichroism spectra of solutions containing different ratios of **(12)** and various DNA: (a) Parallel Q1 + **(12)**; (b) Parallel c-kit1 + **(12)**; (c) Anti-parallel Q1 + **(12)**; (d) Parallel Q4 + **(12)**; (e) Hybrid-type 1 Q1 + **(12)**; (f) D2 + **(12)**.

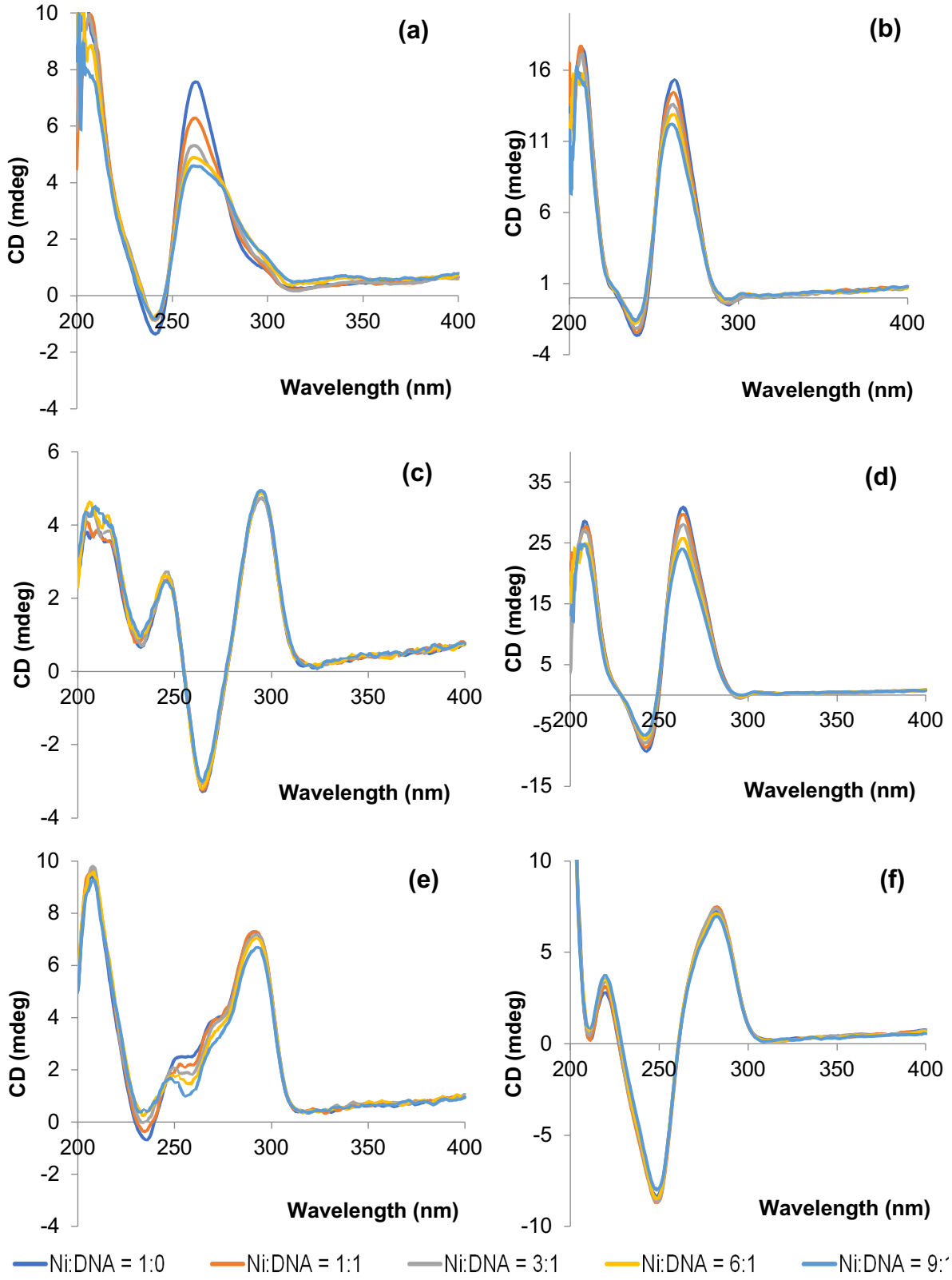

Figure S14e. Circular dichroism spectra of solutions containing different ratios of **(14)** and various DNA: (a) Parallel Q1 + **(14)**; (b) Parallel c-kit1 + **(14)**; (c) Anti-parallel Q1 + **(14)**; (d) Parallel Q4 + **(14)**; (e) Hybrid-type 1 Q1 + **(14)**; (f) D2 + **(14)**.

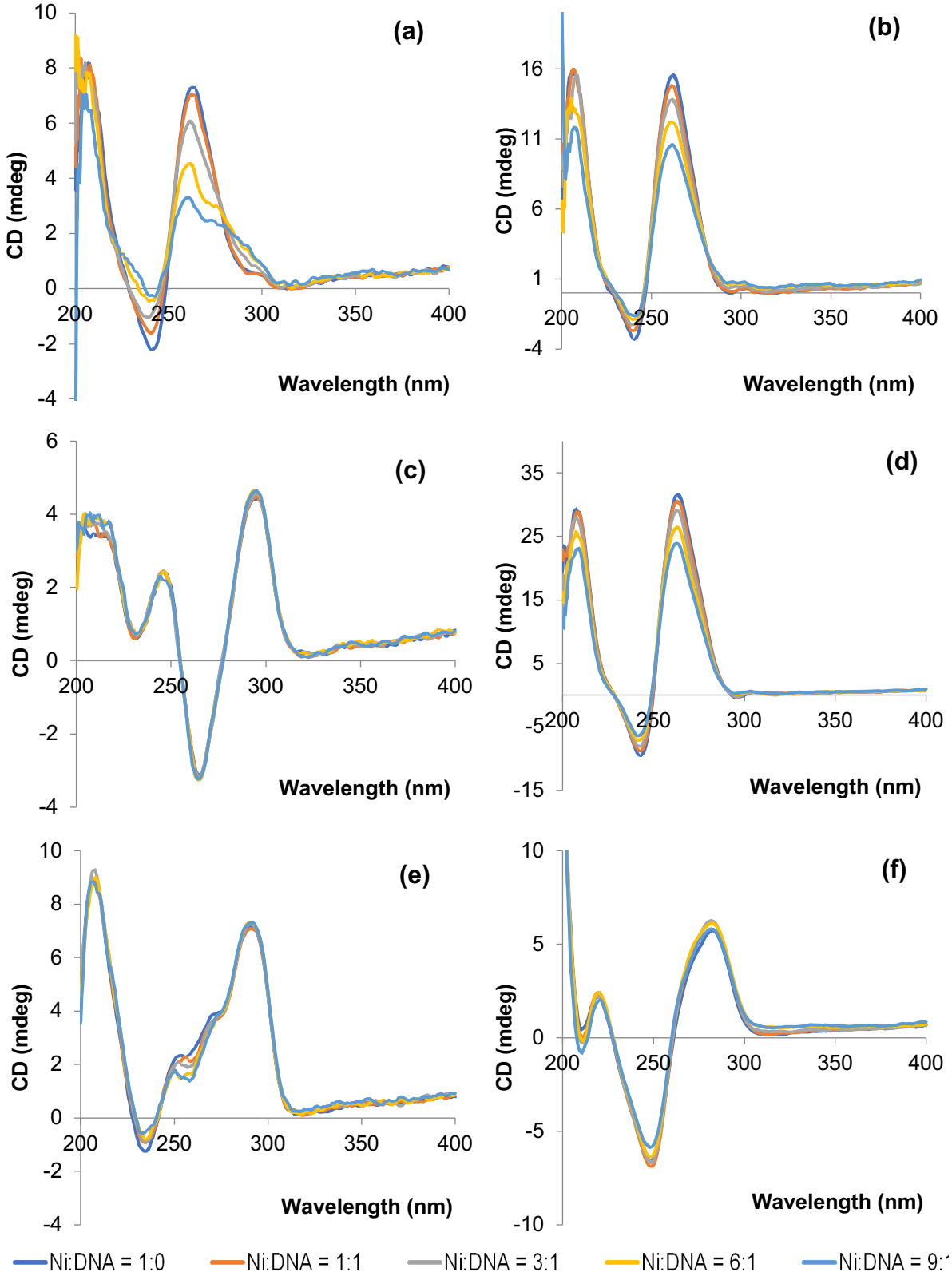

Figure S14f. Circular dichroism spectra of solutions containing different ratios of **(16)** and various DNA: (a) Parallel Q1 + **(16)**; (b) Parallel c-kit1 + **(16)**; (c) Anti-parallel Q1 + **(16)**; (d) Parallel Q4 + **(16)**; (e) Hybrid-type 1 Q1 + **(16)**; (f) D2 + **(16)**.

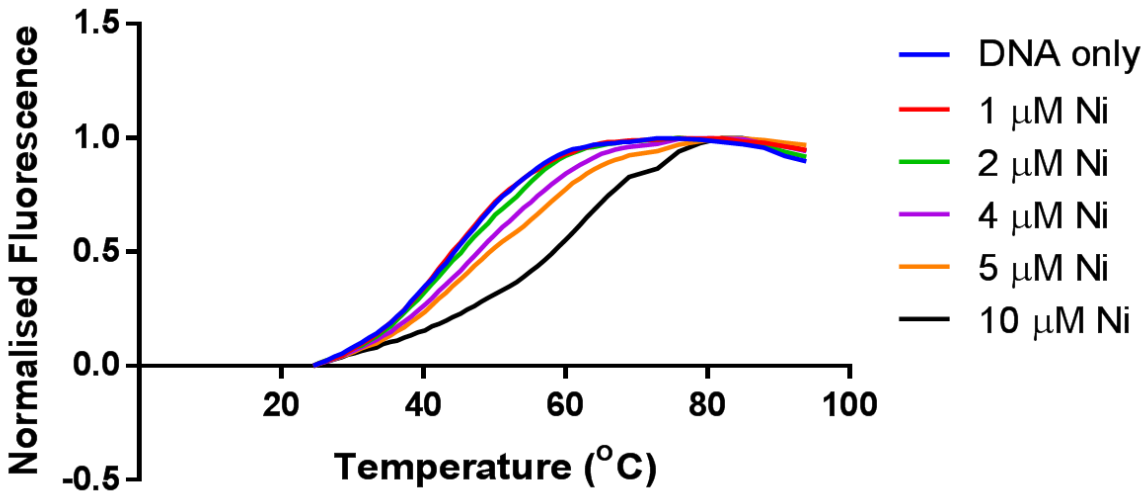

Figure S15a. Normalised FRET melting curves obtained using solutions containing 0.2 μM F21T and different concentrations of **(4)**.

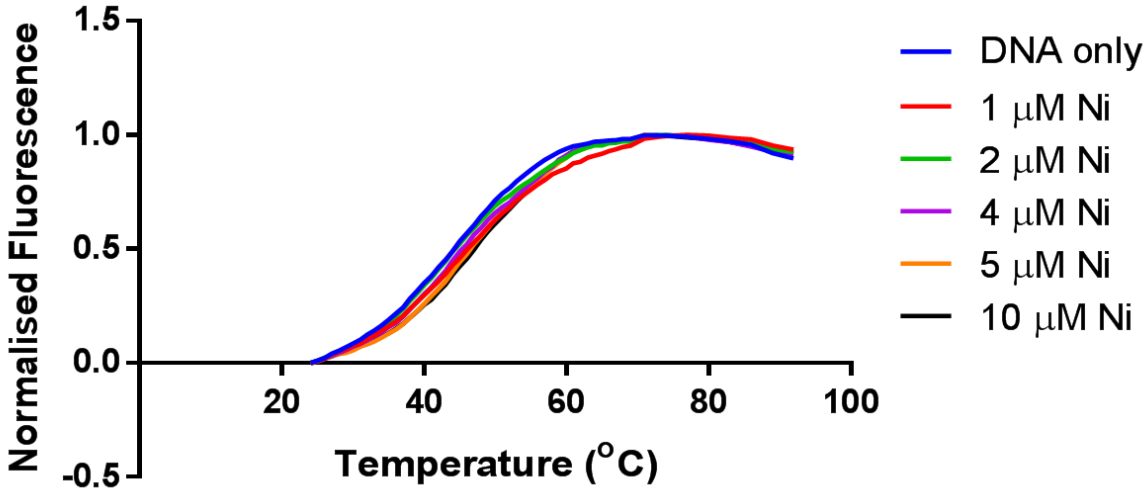

Figure S15b. Normalised FRET melting curves obtained using solutions containing 0.2 μM F21T and different concentrations of **(6)**.

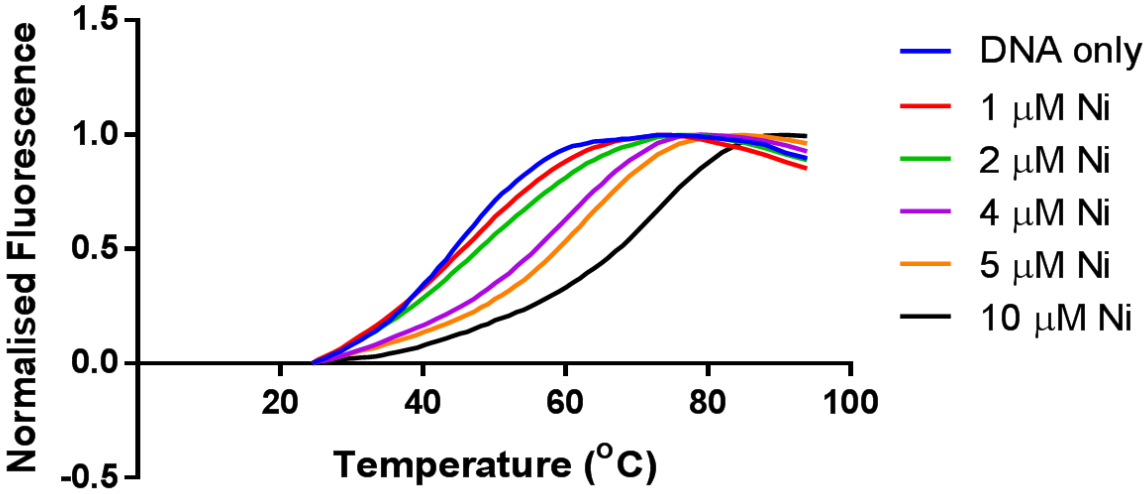

Figure S15c. Normalised FRET melting curves obtained using solutions containing 0.2 μM F21T and different concentrations of **(8)**.

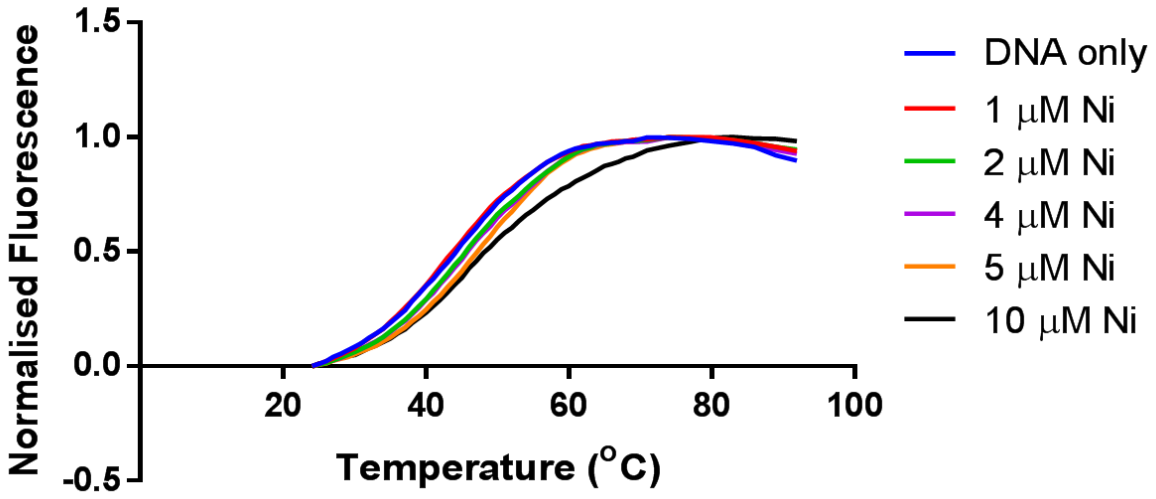

Figure S15d. Normalised FRET melting curves obtained using solutions containing 0.2 μM F21T and different concentrations of **(10)**.

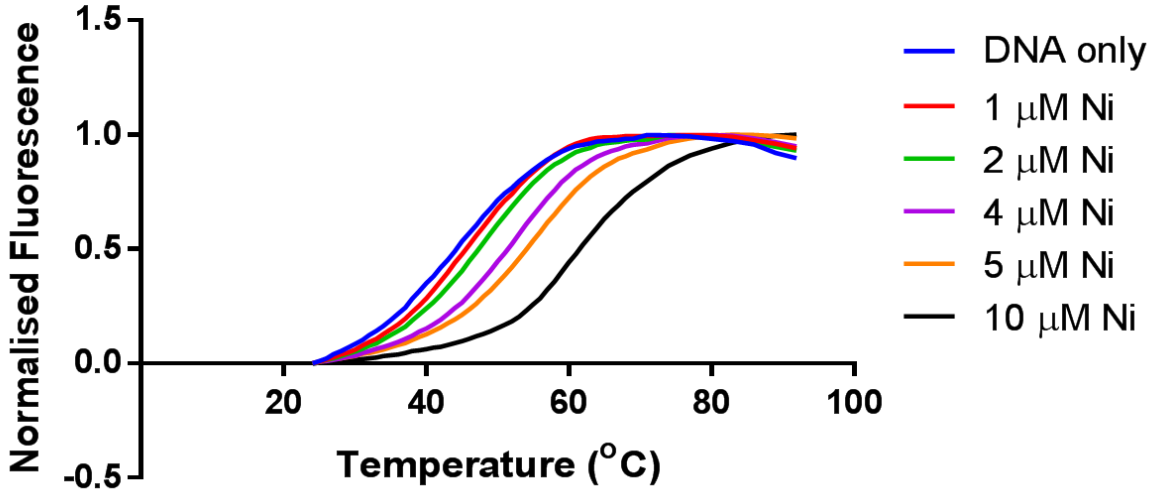

Figure S15e. Normalised FRET melting curves obtained using solutions containing 0.2 μM F21T and different concentrations of **(12)**.

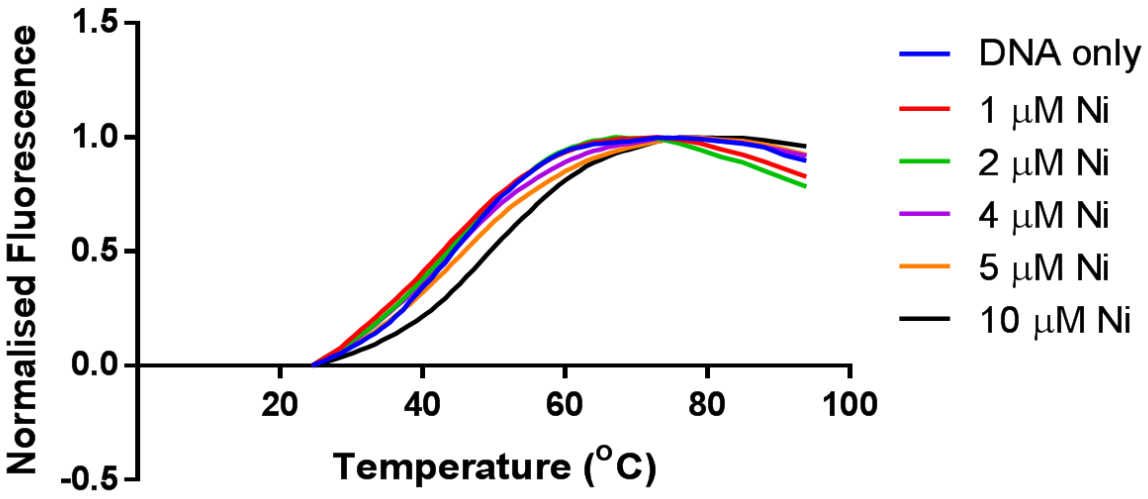

Figure S15f. Normalised FRET melting curves obtained using solutions containing 0.2 μM F21T and different concentrations of **(14)**.

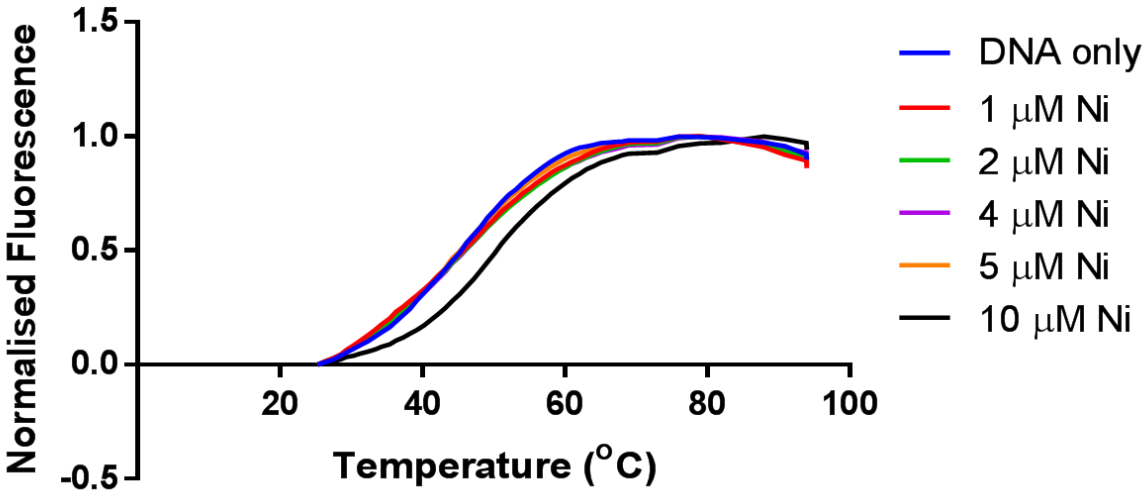

Figure S15g. Normalised FRET melting curves obtained using solutions containing 0.2 μM F21T and different concentrations of **(16)**.

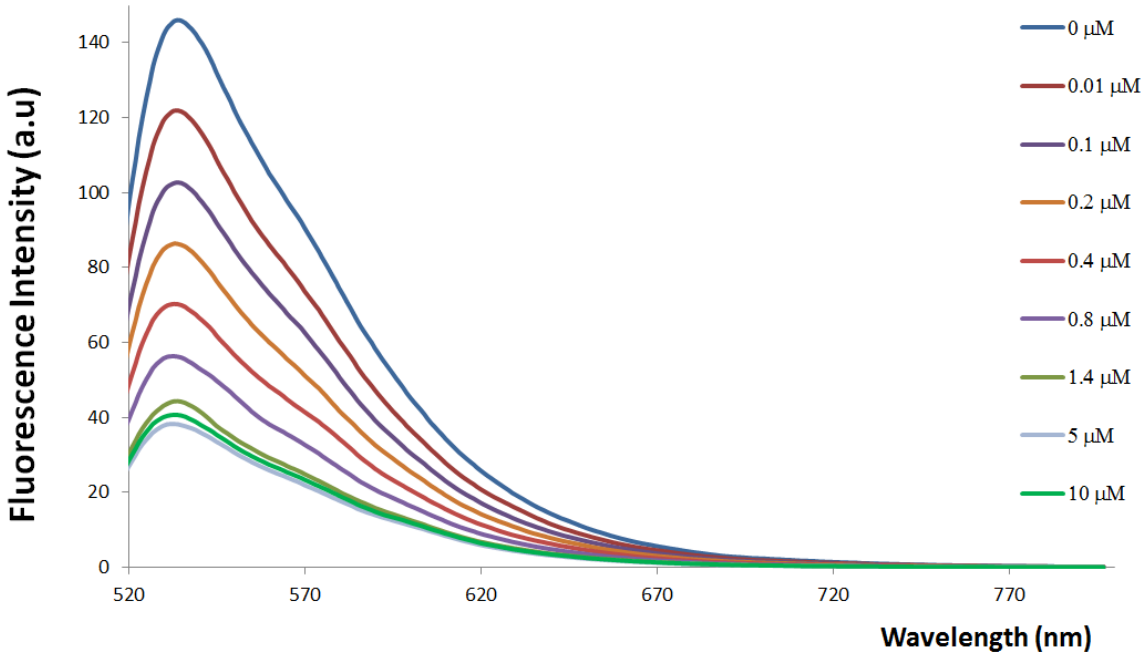

Figure S16a. Fluorescence spectra for solution containing Q1 and TO upon addition of increasing amounts of complex **(4)**.

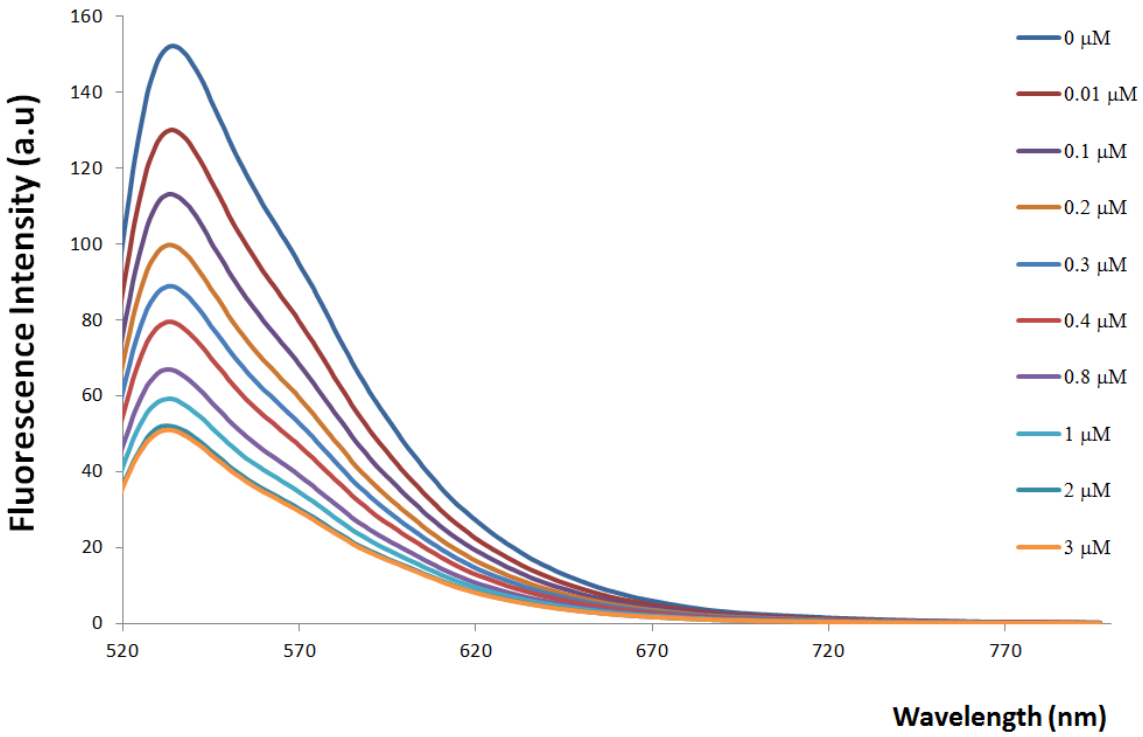

Figure S16b. Fluorescence spectra for solution containing Q1 and TO upon addition of increasing amounts of complex **(6)**.

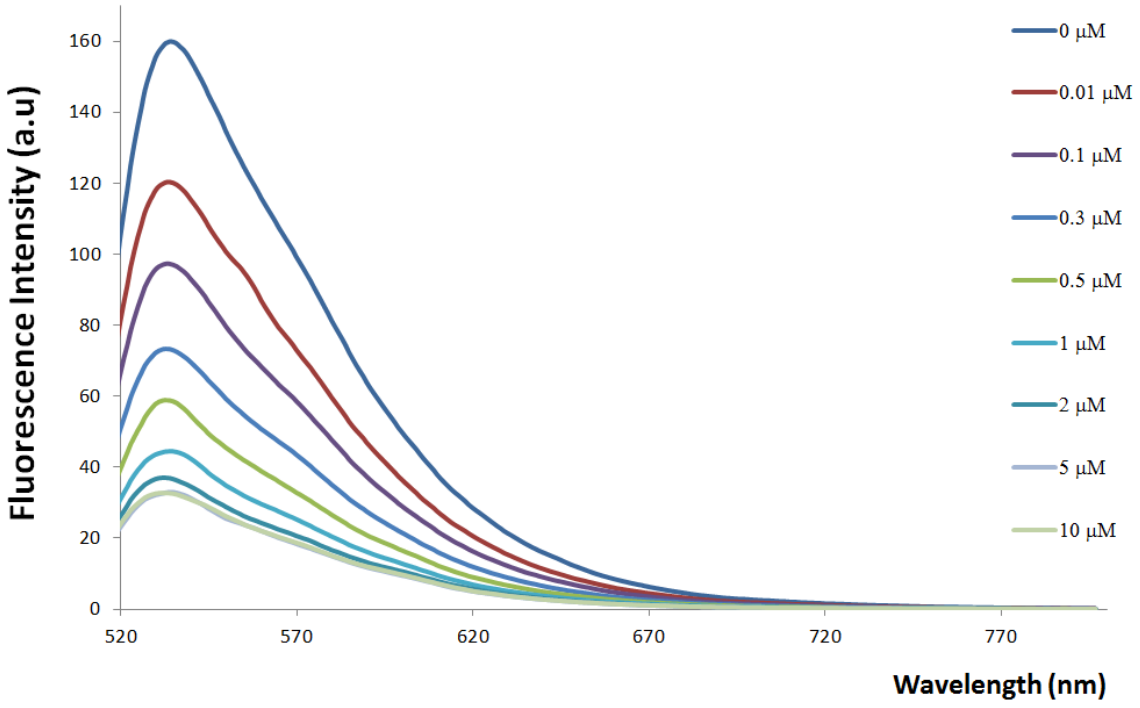

Figure S16c. Fluorescence spectra for solution containing Q1 and TO upon addition of increasing amounts of complex **(8)**.

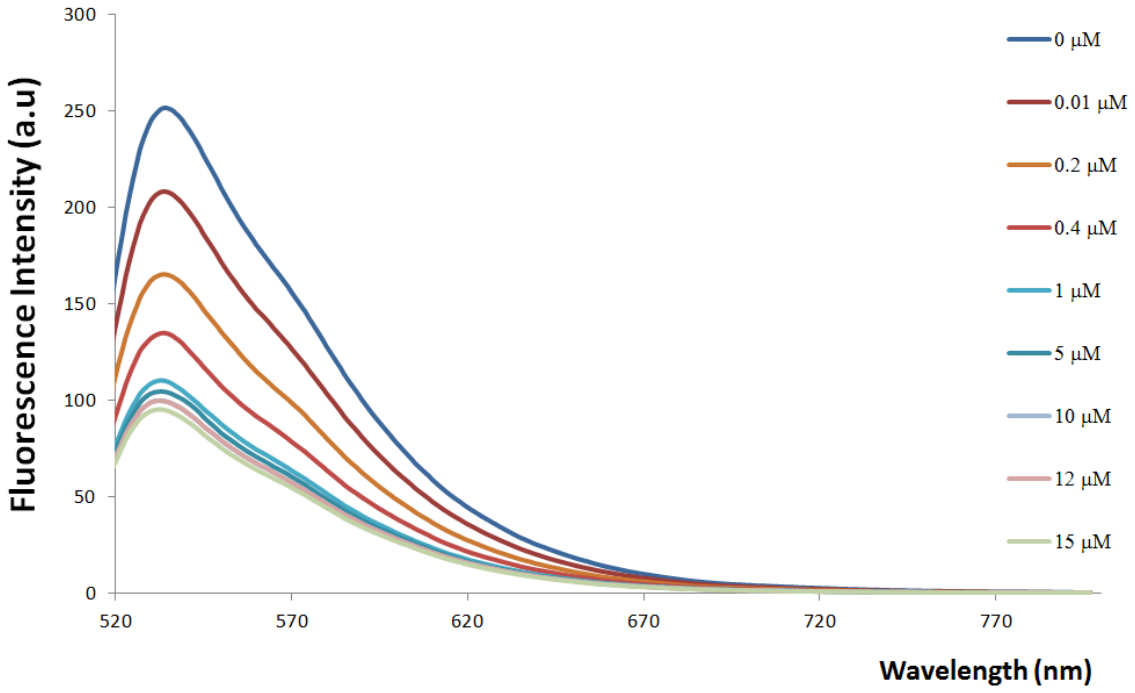

Figure S16d. Fluorescence spectra for solution containing Q1 and TO upon addition of increasing amounts of complex **(10)**.

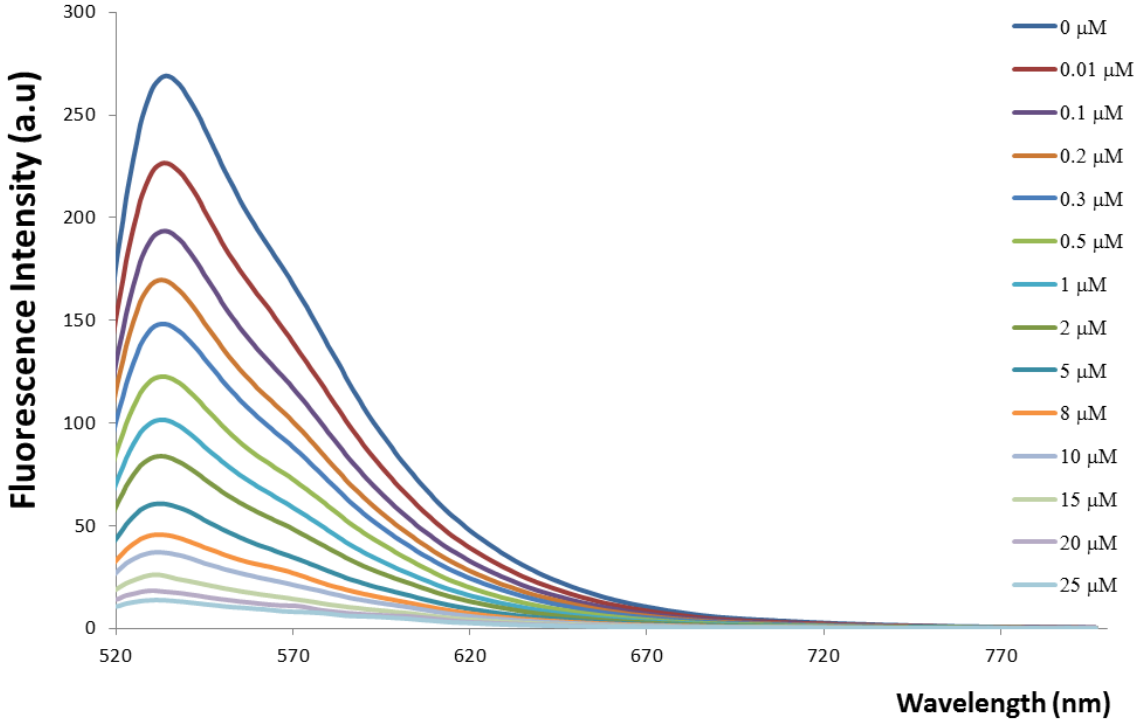

Figure S16e. Fluorescence spectra for solution containing Q1 and TO upon addition of increasing amounts of complex **(12)**.

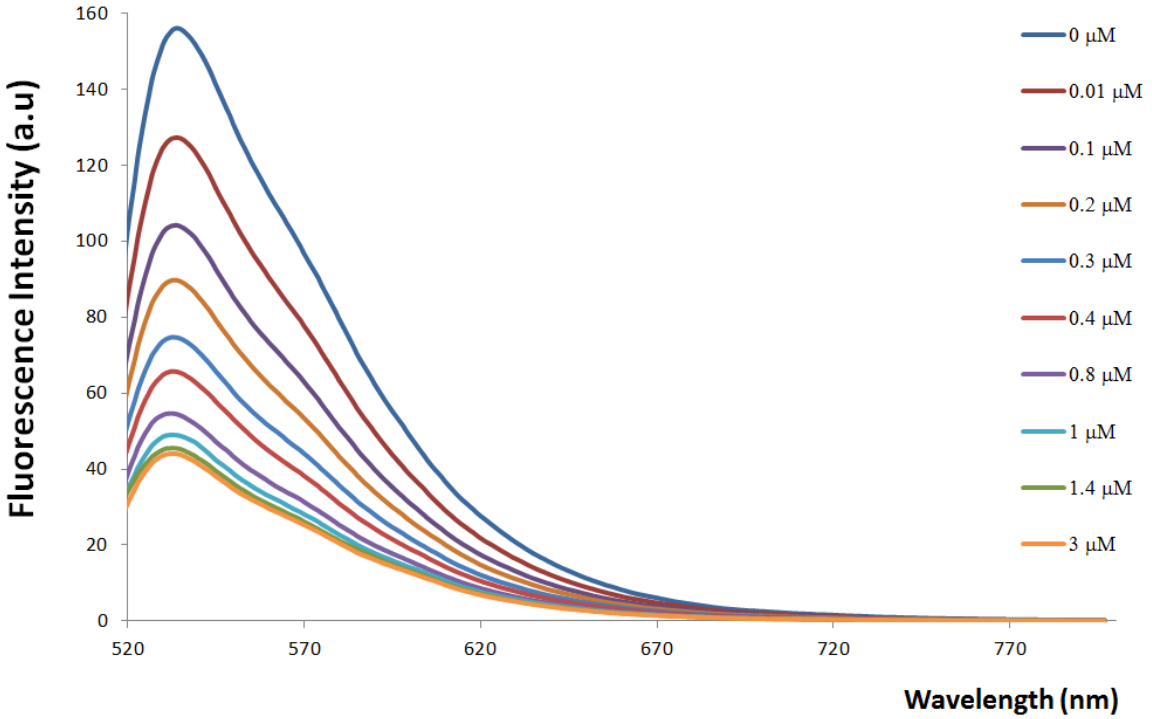

Figure S16f. Fluorescence spectra for solution containing Q1 and TO upon addition of increasing amounts of complex **(14)**.

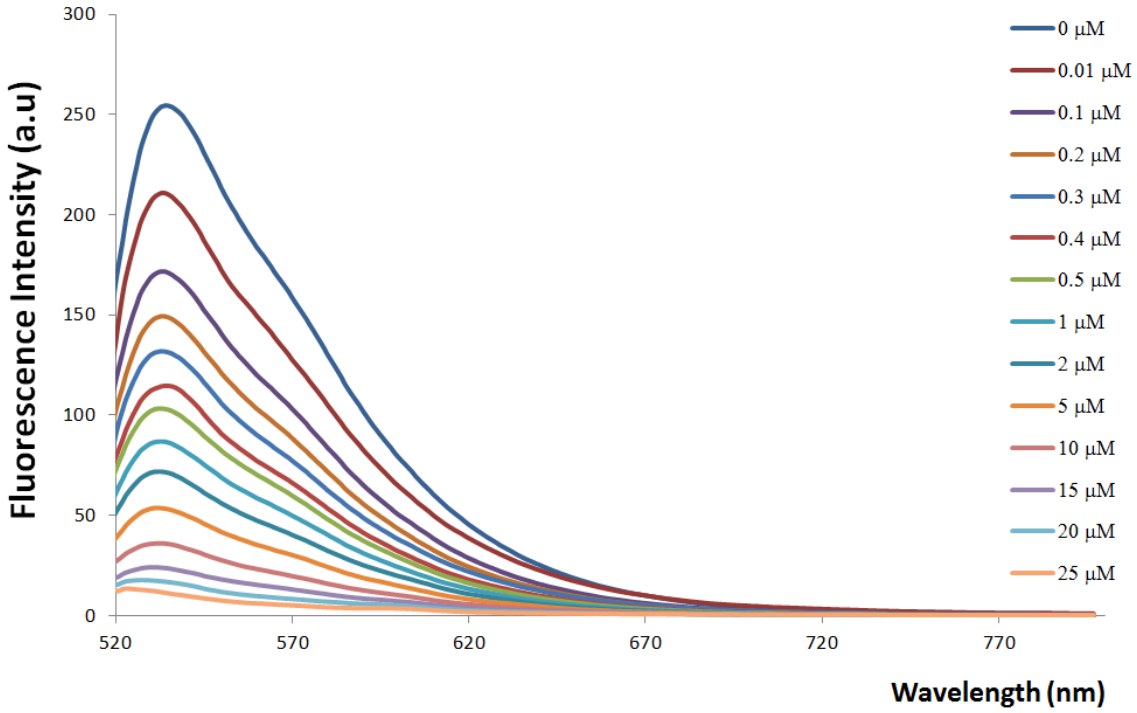

Figure S16g. Fluorescence spectra for solution containing Q1 and TO upon addition of increasing amounts of complex **(16)**.

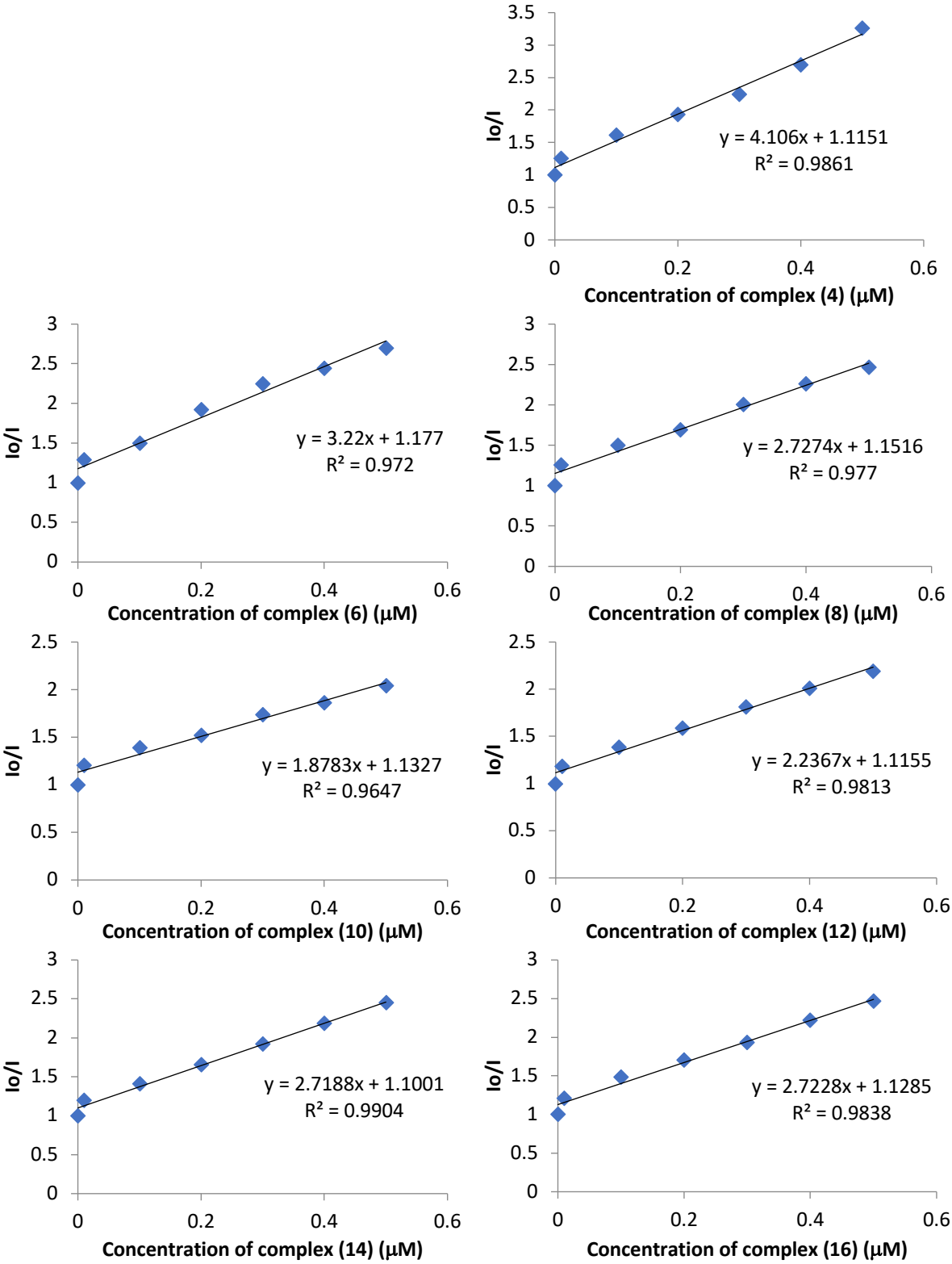

Figure S17. Stern-Volmer plots for FID assays of complexes **(4)**, **(6)**, **(8)**, **(10)**, **(12)**, **(14)** and **(16)** using Q1 and TO.

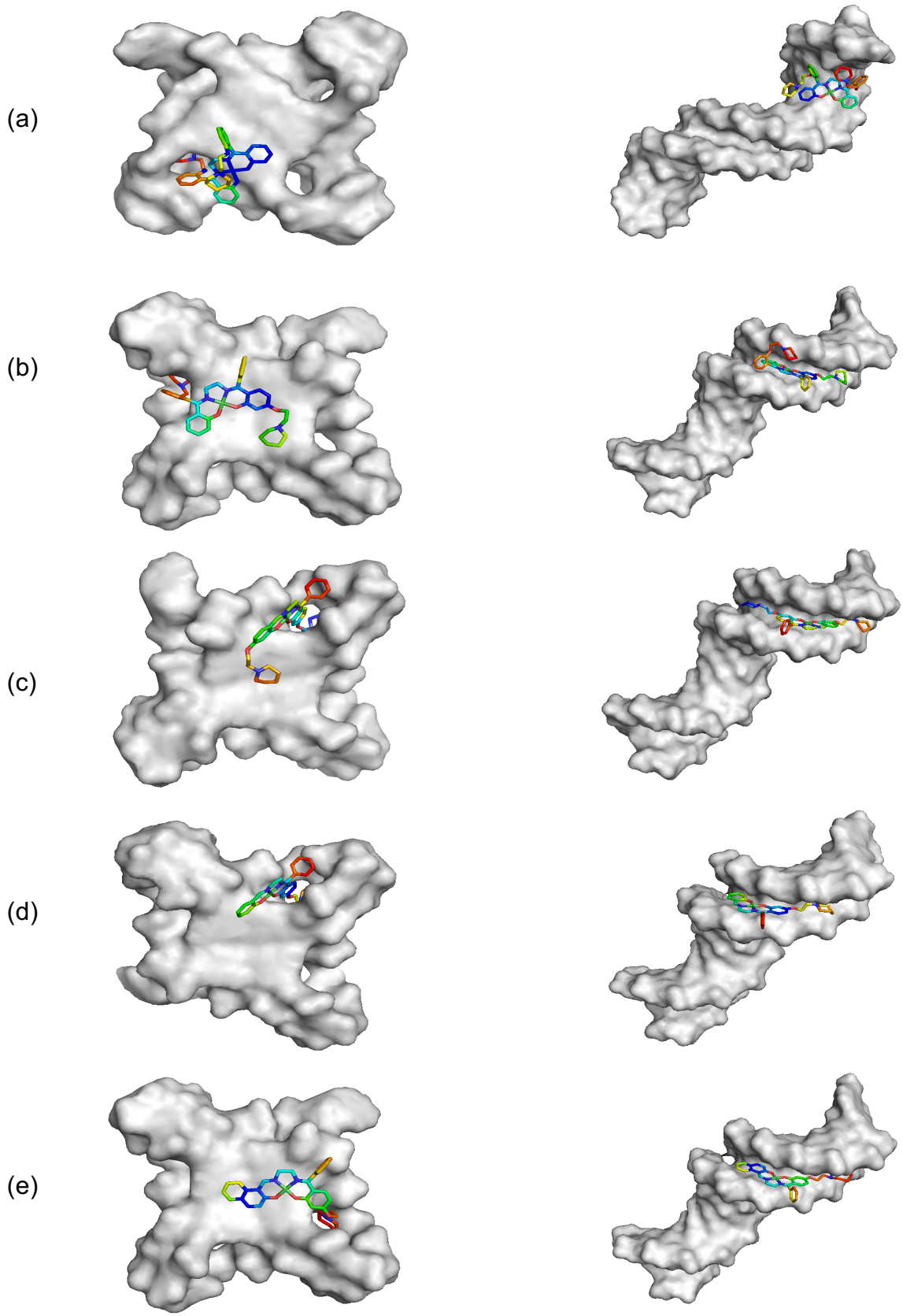

Figure S18. Molecular docking configurations of qDNA 1KF1, dsDNA 1KBD and different complexes. (a) **(6)**, (b) **(10)**, (c) **(12)**, (d) **(14)**, (e) **(16)**, 1KF1 on the left and 1KBD on the right.

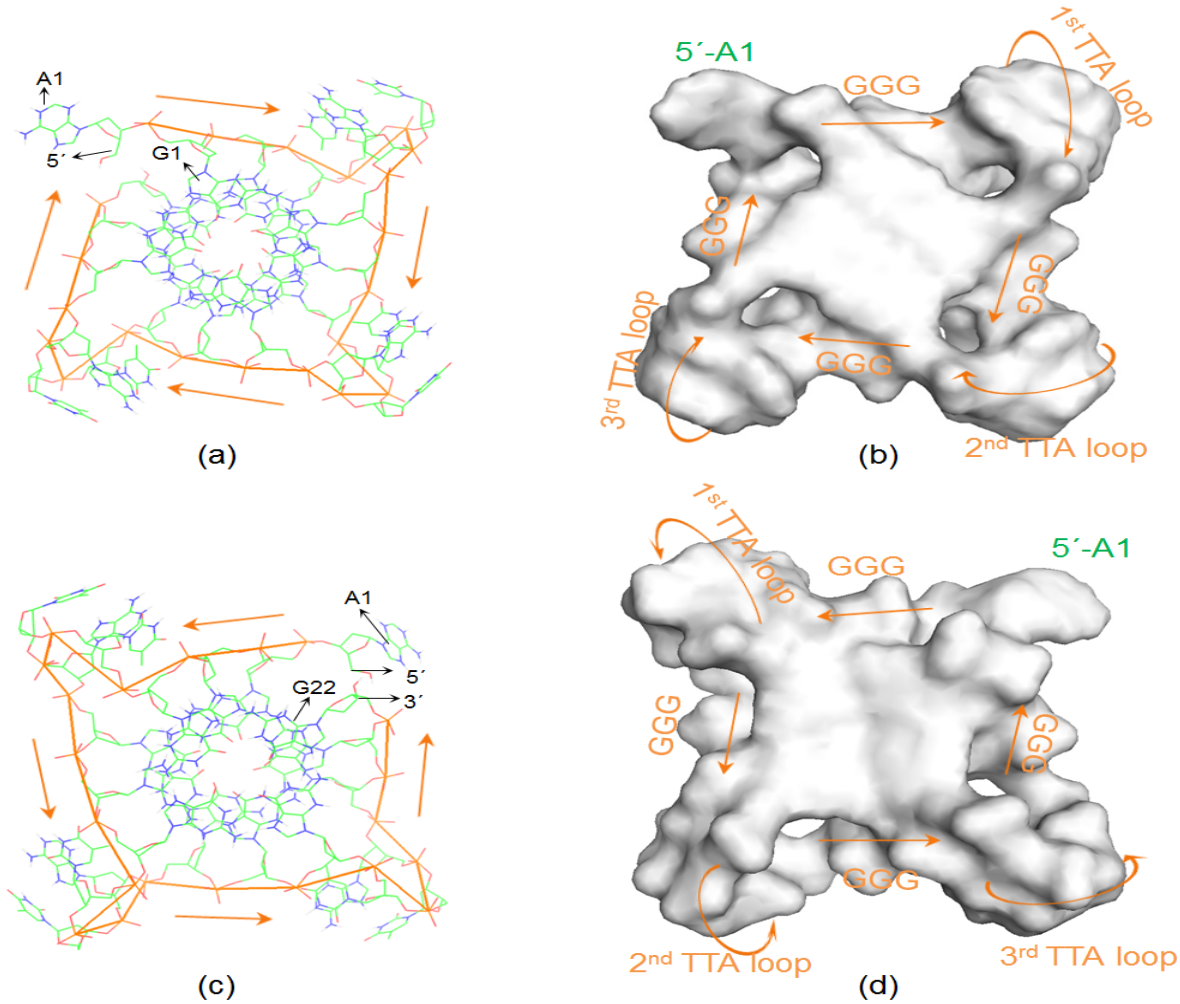

Figure S19. Crystal structure of parallel unimolecular qDNA 5´-AGGG(TTAGGG)$_3$-3´(1KF1). (a) Line cartoon of top view; (b) Surface cartoon of top view; (c) Line cartoon of bottom view; (d) Surface cartoon of bottom view. The arrows showed the direction from 5´ to 3´. For the line cartoons: green: carbon, blue: nitrogen, red: carbon, orange: phosphorus.